Role of Electronic Structure in the Susceptibility of Metastable Transition-Metal Oxide Structures to Transformation

John Reed and Gerbrand Ceder*

Department of Materials Science and Engineering, Massachusetts Institute of Technology, Building 13-5056, 77 Massachusetts Avenue, Cambridge, Massachusetts 02139

Received March 1, 2004

Contents

1. Introduction

Kinetic stability is a key aspect of Li-insertion compounds used in rechargeable Li batteries. To obtain high capacity, the Li ions need to be cycled over a wide range of concentrations within the host structure of the insertion compound. This almost invariably brings the host structure outside its range of thermodynamic stability at some stage of the electrochemical cycle. Maintaining a desirable host structure over repeated electrochemical cycles often hinges upon the host structures resistance against transforming into more stable phases when it becomes thermodynamically metastable. The ability to resist phase transformation can have an important impact on the overall performance of a Li-insertion compound used as an electrode material in a Li rechargeable battery.

The focus of this paper is on the role electronic structure plays in determining the site preference and mobility of 3d transition-metal ions in an oxide and how these factors in turn affect the resistance of metastable 3d transition-metal oxides against transformation. This is a relevant topic to the Li rechargeable battery field because 3d transition-metal oxides are often used as positive electrode materials.

Lithium manganese oxide structures serve as the main prototype of a 3d transition-metal oxide system used in this investigation. Lithium manganese oxides have been intensely researched as candidate positive electrode materials for use in Li rechargeable batteries because they offer the possibility of high capacity combined with good safety. This desirable combination is a consequence of the relative stability of the fully charged MnO_2 structures. Mn is also less expensive than Co, the transition metal commonly used today in positive electrode materials for rechargeable Li batteries.[1]

The Mn oxide structures that have received the most attention as possible positive electrode materials are spinel,[2−4] α-$NaFeO_2$-type layered,[5−9] and orthorhombic (*Pmnm*).[2,3] All three of these structures have a close-packed (sometimes slightly distorted) oxygen array in a fcc-like stacking with Mn occupying octahedral sites and Li occupying either octahedral or tetrahedral sites. Unfortunately, each of these structures has problems that have hindered their practical use in Li rechargeable batteries thus far.[2,3,5,10,11] For the α-$NaFeO_2$-type layered and orthorhombic (*Pmnm*) structures the primary problem is that they undergo structural transformation with electrochemical cycling. As such the Mn oxides are a good prototype for investigating the relationship between transformation kinetics and electronic structure.

One advantage that spinel-like $Li_xMn_2O_4$ (*s*-$Li_xMn_2O_4$) has over the other candidates is that it is not susceptible to any major structural transformation upon electrochemical cycling over the $0 \leq X_{Li} \leq 2$ range.[2] This is due in part to *s*-$Li_xMn_2O_4$ being

* To whom correspondence should be addressed. Phone: (617) 253-1581. Fax: (617) 258 6534. E-mail gceder@mit.edu.

10.1021/cr020733x CCC: $48.50
Published on Web 09/28/2004

John Reed received his Ph.D. degree in Materials Science and Engineering from the Massachusetts Institute of Technology in 2003. Currently he is doing postdoctoral work for the Massachusetts Institute of Technology in addition to being a visiting scientist at Lawrence Berkeley National Laboratory. His current interests are energy technologies and utilization of computational methods to analyze materials used in these technologies, as well as identification of new candidate materials. His primary research focus to date has been on transition-metal oxide materials used in the positive electrodes of Li rechargeable batteries and the physics and chemistry that govern their properties.

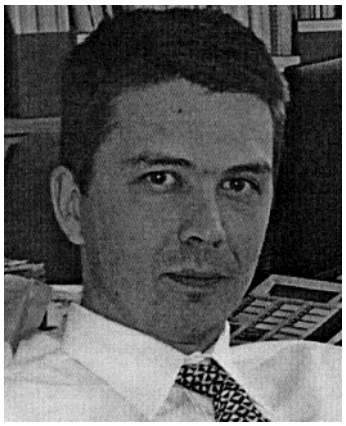

Gerbrand Ceder is the R. P. Simmons Professor of Materials Science and Engineering at the Massachusetts Institute of Technology. He received his engineering degree in Metallurgy and Applied Materials Science from the University of Leuven, Belgium, in 1988, and his Ph.D. degree in Materials Science from the University of California at Berkeley in 1991, at which time he joined the MIT faculty. Ceder's research interests lie in computational modeling of material properties and design of novel materials. He has published over 160 scientific papers in the fields of alloy theory, oxide phase stability, high-temperature superconductors, and Li-battery materials, and holds three current or pending U.S. patents. He has received numerous awards among which a Career Award from the National Science Foundation, the Robert Lansing Hardy Award from The Metals, Minerals and Materials Society for "exceptional promise for a successful career", the 2004 Battery Research Award from the Electrochemical Society, and an award from the graduate students at MIT for best teaching. He has worked with several U.S. and international materials companies to use modeling to design and optimize materials for high-performance applications. He is also a co-founder of Computational Modeling Consultants, which provides first-principles materials modeling services to industry. He is currently head of the Theory and Modeling Division of the Institute for Soldier Nano Technology at MIT and a group leader for the Research Program on High Performance Power Sources in the Center for Materials Science and Engineering.

thermodynamically stable at $X_{Li} = 1$. Additionally s-$Li_xMn_2O_4$ retains its structural integrity at high and low lithiation even though it becomes energetically metastable at those compositions.[2]

The low energy of the spinel structure at the $LiMn_2O_4$ composition is not unique to Mn. For the 3d transition metals from Ti to Cu, the energy of the spinel structure is lower than the energy of the layered structure.[12,13] This is not too surprising since there is a greater separation between neighboring positively charged Li and M cations (M ≡ 3d transition-metal ion) in the spinel structure—where the Li occupy tetrahedral sites and the M octahedral sites—than in the layered structure—where both Li and M occupy octahedral sites.[2]

As mentioned previously, both α-$NaFeO_2$-type layered (l-Li_xMnO_2) and orthorhombic (o-Li_xMnO_2) lose their structural integrity with electrochemical cycling, in contrast to s-$Li_xMn_2O_4$, and rapidly transform to a spinel-like material at partial lithiation.[9,14−17] This results in a substantial drop in capacity over the first few charge/discharge cycles.[8] However, capacity is recovered with additional cycling as the transformation to spinel moves toward completion.[18] The transformed spinel-like material is reported to have properties such as reduced Jahn−Teller distortion and greater durability that are actually superior to conventionally synthesized s-$Li_xMn_2O_4$ spinel.[15,18,19] Nonetheless, there remains an interest in making layered manganates that can resist transforming into spinel.

Although spinel is energetically favored at the $Li_{1/2}MO_2$ composition for all of the 3d transition metals from Ti to Cu, the rate at which the layered structure transforms to spinel varies substantially for each 3d metal. For Li_xMnO_2 the transformation from layered to spinel occurs rapidly at room temperature. In the case of Li_xNiO_2, heating is required in order for layered to rapidly transform to spinel.[20] While for Li_xCoO_2 the transformation of layered to spinel appears to be even more difficult, with the conversion only detected by TEM in the surface layers of highly cycled l-Li_xCoO_2.[21,22] In the following sections the transformation of the layered α-$NaFeO_2$ structure to spinel will be focused upon as an example (with significant relevance to the battery field) that illustrates the influence of electronic structure on the transformation kinetics of 3d transition-metal oxides.

2. Transformation Mechanisms

The transformation of l-Li_xMO_2 or o-Li_xMO_2 into s-$Li_xM_2O_4$ (M ≡ 3d transition-metal ions) does not require oxygen rearrangement since all the structures share a cubic closed-packed (ccp) oxygen anion sublattice. In all three structures M ions occupy octahedral interstitial positions while the Li occupy either octahedral or tetrahedral interstices.[2] Hence, the transformation of l-Li_xMnO_2 or o-Li_xMnO_2 to s-$Li_xMn_2O_4$ involves a rearrangement of Mn from the set of octahedral sites characterizing l-$LiMnO_2$ or o-$LiMnO_2$ to the set of octahedral sites characterizing s-$LiMnO_2$ (as well as rearrangement of the Li ions).

Formation of spinel from l-Li_xMnO_2 requires the movement of one-fourth of the Mn ions from the Mn (111) plane into the Li (111) plane as can be seen by examining Figure 1.

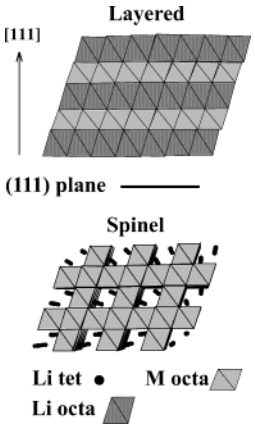

Figure 1. *l*-Li_xMO_2 (layered) and *s*-LiM_2O_4 (spinel) structures (M ≡ 3d transition metal). M occupy octahedral sites in both structures. In *l*-Li_xMO_2, M and Li (and/or vacancies) alternately occupy (111) planes of the ccp oxygen sublattice. The (111) plane parallel to the M layers is indicated by the black line between the layered and spinel structures. The [111] direction is shown as well. In *s*-$Li_{1/2}MnO_2$, (111) planes with three-fourths of the Mn alternate with (111) planes with one-fourth of the Mn. Li ions occupy tetrahedral sites in the planes with one-fourth of the Mn. The planes with three-fourths of the Mn are free of Li. In fully lithiated spinel-like *s*-$Li_2Mn_2O_4$, the Li move into octahedral sites. Three-fourths of the Li are in the (111) plane with one-fourth of the Mn, and one-fourth of the Li are in the plane with three-fourths of the Mn.

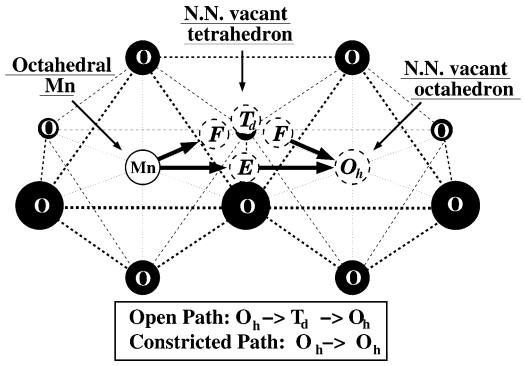

Figure 2. The most direct path an octahedral Mn can follow to a vacant nearest neighbor octahedral site (O_h) is through the edge (*E*) shared by the two sites. This path ($O_h \rightarrow O_h$) is also the most constricted in terms of separation between the migrating Mn and the surrounding oxygen anions. The minimum separation occurs as Mn passes through the center of the octahedral edge labeled *E*. A more open path between octahedral sites is via a nearest neighbor (n.n.) tetrahedral site (T_d). Along this path ($O_h \rightarrow T_d \rightarrow O_h$) the minimum separation between a migrating Mn and surrounding oxygens occurs as Mn passes through the center of the shared triangular face between the n.n. octahedron and tetrahedron (*F*). In a perfect octahedron the distance between the corner oxygens and the center of the triangular face (i.e., distance from **O** to *F*) is 1.155 times the distance from corner oxygens to the center of the edge (i.e., distance from **O** to *E* in Figure 2).

For *o*-Li_xMnO_2, 50% of the Mn ions need to change position in order to form spinel.[2] The characteristics of the orthorhombic, α-$NaFeO_2$-type layered, and spinel structures as well as many other ordered rocksalt structures have been covered in detail by Thackeray.[2]

Given that the structural transformation of the α-$NaFeO_2$-type layered and orthorhombic structures to spinel only requires cation migration, the varying resistance of transition-metal compositions against the transformation (i.e., low resistance for Mn, high for Co) is most likely connected to the diffusion kinetics of the respective 3d transition-metal ions.

An ion can take two extreme paths in migrating between octahedral sites of a ccp oxygen framework, as occurs during the transformation of *l*-Li_xMnO_2 or *o*-Li_xMnO_2 to *s*-$Li_xMn_2O_4$. These two paths are shown in Figure 2. The most direct path travels straight through the edge shared by neighboring octahedra, i.e., the $O_h \rightarrow O_h$ path through *E* shown in Figure 2. This path, while short, brings the cation in close proximity to the coordinating oxygen anions. A more open but longer path is through a nearest neighbor (n.n.) tetrahedral site via the faces (*F*) it shares with the neighboring octahedra (i.e., path $O_h \rightarrow T_d \rightarrow O_h$ in Figure 2).

While the octahedra shown in Figure 2 are undistorted, this is generally not the case in structures such as *l*-Li_xMnO_2 and *o*-Li_xMnO_2. In these cases the octahedra are distorted by both the cationic ordering which breaks the cubic symmetry of the underlying oxygen sublattice and the Jahn−Teller distortion when Mn^{3+} is present. Consequently, not all of the octahedral edges (*E*) or faces (*F*) that Mn can pass through are equivalent in *l*-Li_xMnO_2 and *o*-Li_xMnO_2.

Generally, the activation barrier for a transition-metal ion passing through the triangular oxygen face (*F*) along a $O_h \rightarrow T_d \rightarrow O_h$ type path is expected to be less than the barrier to pass through the oxygen edge (*E*) along a $O_h \rightarrow O_h$ type path. The separation between cation and oxygen is about 15% greater at *F* than at *E* (assuming an undistorted octahedron). Hence, there should be less Pauli repulsion from the electron clouds of the oxygen when the cation passes through the octahedral face (*F*) than when passing through the octahedral edge (*E*). Previous work has shown that Li favors a $O_h \rightarrow T_d \rightarrow O_h$ type path when diffusing in the Li layer of *l*-Li_xCoO_2.[23] It is expected that 3d metal ions will typically take $O_h \rightarrow T_d \rightarrow O_h$ type paths (Figure 2) as well when diffusing through a ccp oxygen framework, such as during the transformation of *l*-Li_xMnO_2 or *o*-Li_xMnO_2 to *s*-$Li_xMn_2O_4$. The results of first-principles calculations discussed in the following sections support this view.

A notable exception to the general favorability of $O_h \rightarrow T_d \rightarrow O_h$ type paths for cation migration is cases where the intermediate tetrahedral site (T_d) shares a face with an octahedral site occupied by another cation. The passage of a 3d metal ion through such tetrahedral sites is typically calculated to be high in energy, in some cases higher than the energy for passing through the octahedral edge (i.e., the $O_h \rightarrow O_h$ path).[24] This is due to the small separation and hence strong repulsion between face-sharing cations in a ccp oxygen framework.

In the following sections it will be shown that first-principles calculations and ligand-field theory indicate that the energetics for the passage of a 3d ion like Mn through intermediate triangular (*F*) and tetrahedral (T_d) sites is highly effected by its oxidation state.[76] This suggests that the kinetics of phase

transformations involving 3d ion rearrangements in a ccp oxygen framework will depend strongly upon oxidation state. Since the maintenance of structural integrity is a desirable feature for an electrode material, the effect of valence on ionic mobility is an important consideration when designing electrodes. For multivalent TM ions it is possible that the TM ion could have a low mobility in one valence,- but a high mobility in another, which could make the host structure vulnerable to transformation during electrochemical cycling.

3. Density Functional Theory

Much of the quantitative information in this paper is derived from first-principles calculations based on density functional theory (DFT).[25−27] Experimentally it is difficult to determine ion migration paths and energy barriers along migration paths in structural transformations such as from *l*-Li_xMnO_2 to *s*-$LiMn_2O_4$. Examining the atomic-scale ionic movements that could occur in such a transformation using first-principles calculations can therefore be informative.

For characteristics of TM oxides such as Li_xMnO_2 or Li_xCoO_2 that can be experimentally determined, it is found that the calculated results presented in this paper are in good agreement with experiment.[77] Additionally, previous studies have found that various properties of 3d TM oxides can be determined with good accuracy using DFT-based methods.[13,28,29] This gives credibility to the findings of this paper which rely upon the rich and precise atomic-scale detail provided by first-principles calculations.

The density functional calculations were performed using the Vienna Ab Initio Simulation Package (VASP).[30] The spin-polarized generalized gradient approximation,[31,32] Perdue−Wang exchange correlation function, and ultrasoft pseudopotentials were used.[33]

Defects can be calculated in supercells that are multiples of the unit cell for the underlying undefected structure (e.g., *l*-$Li_{1/2}MnO_2$). If the supercell is large enough, the periodic images of the defect will have negligible interaction, giving an approximation of an isolated lone defect.

Such an approximation of periodicity was made for the calculations discussed in the next section (section 4). The supercells for these calculations were composed of either 12 or 32 primitive Li_xMO_2 unit cells (M ≡ 3d TM ion; $0 \le x \le 1$) that contained various M defects. The lattice parameters of the supercells were kept constant at the parameters for the undefected structure, while the ionic coordinates were allowed to relax. A $2 \times 2 \times 2$ *k*-point mesh was used for the calculations on the 12-unit supercells and a $1 \times 1 \times 1$ *k*-point mesh for the 32-unit supercells. The primitive Li_xMO_2 unit cells used to construct the super cells had previously been calculated with full relaxation of lattice parameters as well as ionic coordinates.

Later sections will draw upon the results of calculations on *l*-Li_xMO_2, *s*-$Li_xM_2O_4$, and related metastable crystalline structures. For these calculations a $Li_xM_4O_8$ ($0 \le x \le 4$) unit cell and a $4 \times 4 \times 4$ *k*-point mesh were used. Both the lattice parameters and the ionic coordinates were allowed to fully relax.

The bulk of the calculations in this study were performed on Mn oxide structures; however, as a reference, many equivalent calculations were also carried out for Li_xCoO_2 ($0 \le x \le 1$). This system was chosen for comparison with Li_xMnO_2 because in the layered form it is does not undergo significant phase transformations with electrochemical cycling despite becoming energetically metastable relative to spinel at partial lithiation.[34−37] This resistance to transformation has allowed layered Li_xCoO_2 to become the standard positive electrode material for use in commercial Li rechargeable batteries.

Finally, some calculations equivalent to those performed with Mn and Co were carried out for oxides of the other 3d transition metals, from Ti to Cu, to demonstrate some general principles governing this class of materials.

4. Comparison between the Activation Barriers for Co and Mn Migration

Figures 3 and 4 show the energy barriers calculated for Mn and Co movements out of a TM layer octahedron and into the Li/vacancy layer of the layered α-$NaFeO_2$-type structure (recall that the TM cations have to migrate into the Li/vacancy layer for the transformation to spinel). The cation positions used in these calculations follow the $O_h \rightarrow O_h$ (Figure 3) and $O_h \rightarrow T_d \rightarrow O_h$ (Figure 4) type paths shown in Figure 2.

Figure 3 shows the calculated energy barrier for Mn and Co hopping directly through an octahedral edge (*E*) into a Li/vacancy layer octahedron. The barrier illustrated at the top of Figure 3 is the calculated result when the Li content is $X_{Li} = 0$ (i.e., MO_2, M ≡ Mn or Co); the bottom plot corresponds to

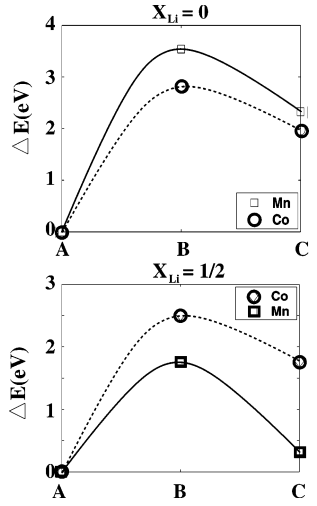

Figure 3. Energy of Co/Mn ion along the $O_h \rightarrow O_h$ transition path from an octahedral site in the TM layer, through a shared edge, to an octahedral site in the vacancy/Li layer: (top) delithiated $X_{Li} = 0$ (M^{4+}), (bottom) half-lithiated $X_{Li} = 1/2$ (average $M^{3.5+}$). (A (on *x* axis)) Layered structure with no transition metal in the empty/lithium layer (i.e., no defects). (B) A single TM atom located in the shared edge between neighboring octahedra (i.e., *E* in Figure 2). (C) A single TM atom defect in an empty/lithium layer octahedron.

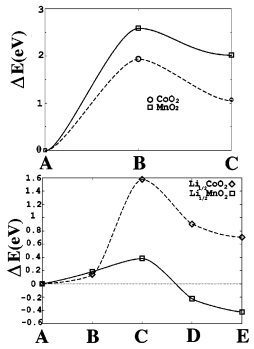

Figure 4. Energy for a Mn/Co ion along the path from an octahedral site in the TM ion layer to a tetrahedral site in the Li/vacancy layer. (top) Delithiated MO_2 (M ≡ Mn or Co: (A) layered structure, (B) single TM ion located in triangular face between TM layer and empty layer (i.e., *F* in Figure 2), (C) single tetrahedral TM defect in empty layer. (bottom) Half-lithiated, i.e., $Li_{1/2}MO_2$: (A) layered structure, (B) Li disorder to create a trivacancy around a tetrahedron in the Li layer (prevents high-energy face-sharing cations for tetrahedral defect), (C) single TM ion located in triangular face between TM layer and Li layer, (D) single tetrahedral TM defect in Li layer, (E) both Li and TM ion in tetrahedral sites (tetrahedral site available to Li due to vacancy created by TM defect).

a Li content of $X_{Li} = 1/2$. The TM ion hop in both cases is along the "constricted" $O_h \rightarrow O_h$ path shown in Figure 2 and results in the formation of an octahedral Mn or Co defect in the Li/vacancy layer.

Figure 4 shows the calculated energy barrier for Mn and Co hopping through an octahedral face (*F*) into a nearest neighbor tetrahedron in the Li/vacancy layer at $X_{Li} = 0$ and 1/2. This path is the first half ($O_h \rightarrow T_d$) of the "open" $O_h \rightarrow T_d \rightarrow O_h$ path pictured in Figure 2.

Figures 3 and 4 catalog the plausible initial steps in the transformation of the layered structure to spinel. Other $O_h \rightarrow O_h$ and $O_h \rightarrow T_d \rightarrow O_h$ cation hops within the transition-metal layer have also been calculated, but they were found to be particularly high in energy due to cationic repulsion and hence are ruled out.[24]

As expected, the barrier is calculated to be lower (at a given lithium content) for hops from octahedra to n.n. tetrahedra through a shared face ($O_h \rightarrow T_d$) than hops directly between octahedra through an octahedral edge ($O_h \rightarrow O_h$). This is consistent with experimental results that indicate Mn migrates through tetrahedral sites during the transformation of orthorhombic or layered Li_xMnO_2 into spinel.[17,38]

Some additional noteworthy features of the calculated results shown in Figures 3 and 4 are as follows.

(i) The barrier for the TM ion to leave its site in the TM layer is high for both Co and Mn at MO_2 composition.

(ii) The formation energy of a tetrahedral Mn defect in the layered structure at $X_{Li} = 1/2$ is negative, while it is positive for Co.

(iii) The activation barriers for Mn migration are higher than those for Co at $X_{Li} = 0$, but they are much lower at $X_{Li} = 1/2$.

The relatively low energy for Mn migration out of the TM layer and into n.n. tetrahedra in the Li/vacancy layer at $X_{Li} = 1/2$ is probably the Achilles heel of the *l*-Li_xMnO_2 material. It suggests that Mn can easily move out of the layered configuration into the Li/vacancy layer at this composition. This should facilitate the rapid transformation of *l*-$Li_{1/2}MnO_2$ to *s*-$LiMn_2O_4$ since Mn ions need to move from the TM layer to the Li/vacancy layer during the transformation. The results of additional calculations, for example, on the second half of the of the $O_h \rightarrow T_d \rightarrow O_h$ path, reported elsewhere further attest to the relative ease for Mn to move between octahedral and tetrahedral sites along the reaction path toward spinel at $X_{Li} = 1/2$ in *l*-Li_xMnO_2.[24]

Co by contrast is seen in Figures 3 and 4 to have high-energy barriers at both delithiated and partially lithiated compositions along either type of pathway ($O_h \rightarrow T_d \rightarrow O_h$ or $O_h \rightarrow O_h$) into the Li/vacancy layer. Results of TM ion defect calculations at full lithiation, i.e., $X_{Li} = 1$, which are not shown,[76] indicate that both Co and Mn are prevented from entering the Li layer by the lack of octahedral lithium vacancies.

The calculated low activation barrier and defect energy for Mn going $O_h \rightarrow T_d$ at partial lithiation is consistent with the lack of stability of *l*-Li_xMnO_2 against transformation into spinel observed experimentally. Likewise, the high activation barriers for all possible Co hops out of the TM layer are consistent with the relative stability observed experimentally for layered Li_xCoO_2.

Figures 3 and 4 illustrate that TM ion defect energies and activation barriers to forming defects appear to be highly sensitive to the Li concentration in the layered structure. The relative stability of Mn and Co in the TM layer octahedra changes dramatically with increasing Li content, with Mn calculated to be more stable than Co at $X_{Li} = 0$ and far less stable at $X_{Li} = 0.5$. The next section will show that as the average oxidation state of the TM ions changes from +4 to +3.5, due to the Li content changing from $X_{Li} = 0$ to 0.5, different charge-transfer reactions accompany tetrahedral defect formation for Mn as well as for Co. This provides an explanation for the qualitative change in Mn behavior compared to Co and highlights the important role that electronic structure plays in the mobility of these ions.

5. Valence of Co and Mn during Migration

Figures 3 and 4 indicate a significant variation in the Mn and Co migration barrier along the $O_h \rightarrow T_d \rightarrow O_h$ and $O_h \rightarrow O_h$ paths as the oxidation state changes.

Using the calculated electron spin density, the ionic valences can be determined by integrating the electron spin density in a sphere about the ionic centers. Integrating spin density provides the net spin associated with a given TM ion. This captures the formal valence of the cation better than integrating the charge density because it distinguishes the partially filled 3d orbitals of the transition-metal cation from the filled p orbitals of the coordinating oxygens. With this method it is possible to detect the charge-transfer and/or bonding changes that occur for a TM ion as it moves along its migration path.[39,40]

The results of such spin integrations are shown in Figure 5 for Co (top) and Mn (bottom) in various

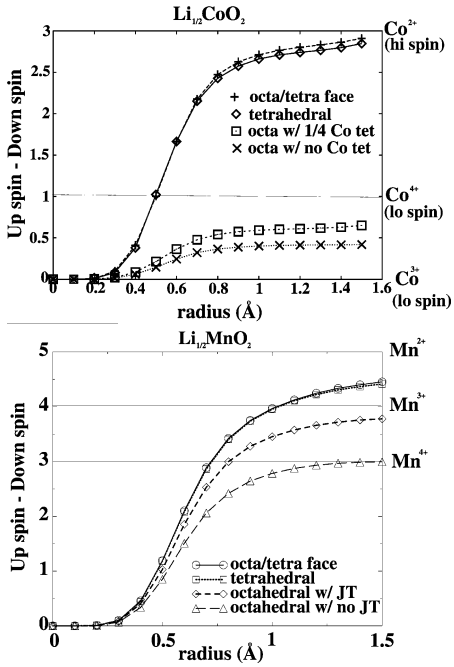

Figure 5. Integrated net spin for Co and Mn cations along the $O_h \rightarrow T_d$ path into the Li/vacancy layer at $X_{Li} = 1/2$. (top) $Li_{1/2}CoO_2$ layered O_h Co ions (labeled octa w/no Co tet) have an oxidation state of $\sim$+3.5 ($t_{2g}^{5.5}$). The migrating Co in triangular (octa/tetra face) or tetrahedral coordination takes on nearly 3 units of electron spin ($1/2\mu_\beta$), giving an oxidation state approaching +2 ($e^4t_2^3$). When one-fourth of the Co are in T_d sites with +2 charge, the other three-fourths of the Co in O_h sites (octa w/1/4 Co tet) have a raised oxidation state from $\sim$+3.6 to +3.7. (bottom) $Li_{1/2}MnO_2$: The migrating Mn (octa/tetra face and tetrahedral) has about 4.5 units of electron spin, giving an oxidation state of $\sim$+2.5 ($e^2t_2^{2.5}$). Mn in Jahn−Teller-distorted octahedra (octahedral w/JT) are $\sim$+3 ($t_{2g}^3e_g^1$); in non-Jahn−Teller-distorted octahedra (octahedral w/no JT) they are +4 (t_{2g}^3).

positions along the $O_h \rightarrow T_d \rightarrow O_h$ path at $t_{Li} = 1/2$. Figure 5 shows the amount of electron spin (in units of $1/2\ \mu_\beta$) as a function of integration radius. The total spin initially rises rapidly with radius as the d orbitals are integrated over. However, then the spin levels off as the nonpolarized oxygen states are reached. The value at this plateau is used in determining the formal valence of the TM cations. For example, the bottom of Figure 5 shows Mn^{4+} which plateaus at a total electron spin of 3, reflecting the $t_{2g}^3e_g^0$ d-orbital filling of Mn^{4+}.

Even though the average formal valence state of the TM is +3.5 at $X_{Li} = 1/2$, Figure 5 shows that the migrating Mn (Co) ion in triangular or tetrahedral coordination takes on quite a different valence from the surrounding octahedral Mn (Co) ions. The migrating Mn (Co) ion gains d electrons when it passes through the triangular octahedron face and keeps them as it continues into the neighboring tetrahedral site in the Li/vacancy layer.

The spin integration results of Figure 5 indicate that when forming a tetrahedral Mn (Co) defect at $X_{Li} = 1/2$, the migrating Mn (Co) approaches a +2 valence state while a neighboring octahedral Mn (Co) is oxidized toward +4. This constitutes a charge-disproportionation reaction which can be approximately expressed by the following equation (where M_{tet}^{2+} is the migrating TM ion)

$$2M_{oct}^{3+} \rightarrow M_{tet}^{2+} + M_{oct}^{4+} \quad (1)$$

A similar charge disproportionation reaction is reported to occur during the degradation of *s*-$Li_xMn_2O_4$ with electrochemical cycling whereby the Mn^{2+} dissolves into the electrolyte.[2]

Using the spin integration method described above, it was also determined that at an average formal valence of +4 ($X_{Li} = 0$) both Mn and Co undergo a simple tetrahedral defect reaction

$$M_{oct}^{4+} \rightarrow M_{tet}^{4+} \quad (2)$$

6. Ligand-Field Effects on the Energetics of Migrating Co and Mn

Size effects are often an important contribution to the energy of ionic systems. However, surprisingly cation size appears to have little if any effect on the propensity of Mn or Co to enter tetrahedral coordination in the Li_xMO_2 ccp oxide system. According to Pauling's first rule, a smaller cation should be more energetically favorable in a small interstitial site than a larger cation.[41] The tetrahedral sites formed by oxygen anions in a ccp structure are smaller than the octahedral sites, so by Pauling's first rule smaller cations should have a greater propensity to enter tetrahedral coordination than larger cations. However, the behavior of the Li_xMnO_2 and Li_xCoO_2 systems is very different than what is expected according to Pauling's first rule.

On the basis of cationic radii reported in the scientific literature (53 pm for Co_{oct}^{4+} and 40 pm for Co_{tet}^{4+}; 53 pm for Mn_{oct}^{4+} and 39 pm for Mn_{tet}^{4+}),[42] one would expect the tetrahedral defect energies and activation barriers for MnO_2 and CoO_2 to be roughly the same. However, as seen previously, the calculated energy for the tetrahedral Mn^{4+} defect is almost twice as high as that of Co^{4+}. The activation barrier for the octahedron−tetrahedron hop is also significantly higher for Mn^{4+} (Figure 4 top).

For the composition $Li_{1/2}MO_2$ (M ≡ Co, Mn), the relevant cations to consider are M^{2+} in tetrahedral coordination, M^{3+} in octahedral coordination, and M^{4+} (given above) in octahedral coordination (58 pm for Co_{tet}^{2+} and 54.5 pm for Co_{oct}^{3+}; 66 pm for Mn_{tet}^{2+} and 64.5 pm for Mn_{oct}^{3+}).[42]

The radius of Co is less than or equal to the radius of Mn at all oxidation states and coordinations relevant to the $Li_{1/2}MO_2$ composition. However, as discussed in the previous section, Mn^{2+} is calculated to be more energetically favored in tetrahedral coordination and have a lower activation barrier for the $O_h \rightarrow T_d$ hop than Co^{2+}, despite being the larger cation.

Finally, according to Pauling's first rule one would expect lower tetrahedral defect and activation barrier energies in MO_2 than in $Li_{1/2}MO_2$ for both Co and Mn since the +4 cations have smaller radii than the +2 cations. Again, site-occupancy predictions based on Pauling's first rule run contrary to the results calculated from first principles.

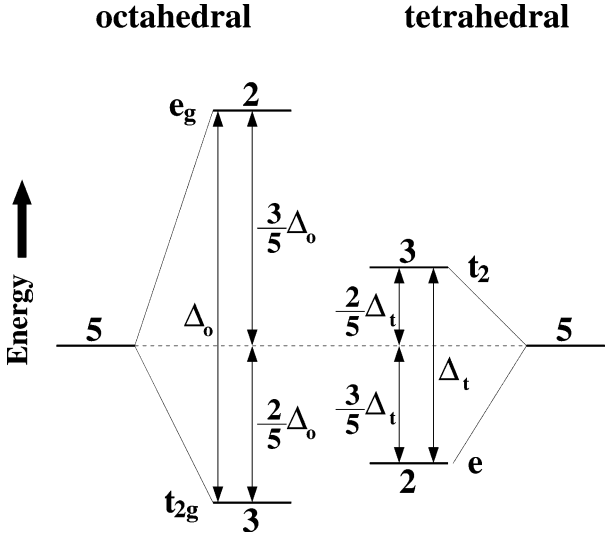

Figure 6. Energy splitting of the d orbitals in octahedral and tetrahedral coordination. The numbers at each level indicate the energy degeneracy that still remains after ligand-field splitting. Note that the energy barycenter (i.e., "center of energy") need not be the same in octahedral and tetrahedral coordination as pictured.

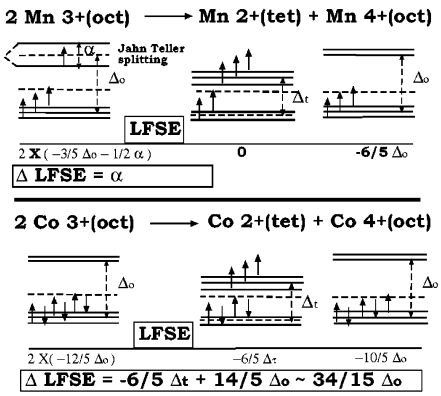

Figure 7. Change in LFSE associated with the charge disproportionation reaction in both $Li_{1/2}MnO_2$ (high-spin Mn^{3+}) and $Li_{1/2}CoO_2$ (low-spin octahedral Co). Δ_o and Δ_t equal the octahedral and tetrahedral ligand-field energy splittings, respectively. The Jahn−Teller splitting equals α. The proportionality between Δ_o and Δ_t is taken from crystal-field theory to be $-4/9\Delta_o = \Delta_t$.[46] Note that the energy barycenter (dashed line) is drawn as a constant, but this is not generally the case nor does it affect the change in LFSE (although it certainly affects the change in total energy).

It appears that for the layered Mn and Co oxides considered, ionic size effects do not play a significant role in the preference for octahedral or tetrahedral sites nor in the activation barrier to hops between the two. Consequently, size effects probably do not play a significant role in determining the mobility of Mn or Co through a ccp oxide framework. In contrast, the results indicate that valence and electronic structure are more decisive factors in the site preference of Mn or Co and hence in their propensity to migrate through a ccp oxide framework. This is consistent with the work of Goodenough that found valence to be an important determinant of the site preference of 3d TM ions in oxides.[43]

The role of electronic structure in Mn and Co site preference and mobility can to some extent be understood through ligand-field theory (LFT).[44,45] LFT qualitatively explains how the degeneracy of the 3d orbitals is broken when a free TM ion is surrounded by coordinating anions. The ligand-field splitting of d orbitals in octahedral and tetrahedral coordination is pictured in Figure 6.[45]

In octahedral coordination, the d level splits into the e_g level, which is 2-fold degenerate, and the t_{2g} level, which is 3-fold degenerate. The energy separation between the t_{2g} and e_g levels is called the ligand-field splitting ($\equiv \Delta_o$). The t_{2g} level, composed of the d_{yz}, d_{xy}, and d_{xz} orbitals modified by the octahedral ligand field, is lowered $(2/5)\Delta_o$ relative to the energy barycenter, i.e., "center of energy", of the d orbitals. The e_g level, composed of the d_{z2} and d_{x2-y2} orbitals, is raised $(3/5)\Delta_o$.[45]

For d orbitals placed in tetrahedral coordination, the t_2 level contains the d_{yz}, d_{xy}, and d_{xz} orbitals modified by the tetrahedral ligand field and the e level contains the d_{z2} and d_{x2-y2} orbitals. Figure 6 illustrates how the energy levels in tetrahedral coordination are inverted relative to those in octahedral coordination (Figure 6).

Using LFT, the change in the ligand-field stabilization energy (LFSE) for the charge disproportionation reaction (eq 1) can be estimated for Mn and Co as shown in Figure 7.

The change in LFSE for the charge disproportionation reaction that produces tetrahedral Mn at $X_{Li} = 1/2$ is projected to be equal to the energy of the Jahn−Teller splitting (α). For Co, on the other hand, the change in LFSE is projected to be more than twice the energy of the octahedral ligand-field splitting ($34/15\Delta_o$), which should be much larger than the Mn Jahn−Teller splitting α.[47,48] Hence, LFT indicates that charge disproportionation is much more costly in ligand-field stabilization for Co than for Mn at $X_{Li} = 1/2$. This is consistent with a much lower mobility for $Co^{3.5+}$ than Mn^{3+} in a ccp oxide and therefore a greater resistance of metastable Co oxides such as *l*-$Li_{1/2}CoO_2$ against transformation. Experimental evidence supporting the decisive role LFSE plays in the differing stability of the layered structures incorporating Mn, Co, as well as Ni has been reported by Choi, Manthiram et al.[49]

It should be kept in mind that while LFSE is important, it is one of many contributions to the energy in the Li_xMnO_2 and Li_xCoO_2 systems. For example, the d levels in Figure 7 are drawn with a constant center of energy, or barycenter (indicated by the dashed line), but this is not generally the case. Hence, in addition to a change in the splitting of the d levels with changing coordination, there can be a shift in their average energy.

Also, the change in LFSE does not account for the energy cost of spin pairing (two electrons with opposing spin occupying the same orbital).[50,51] This is not relevant for Mn in this case, but for Co the change in LFSE of the charge disproportionation reaction is probably somewhat counteracted by the change in spin pairing energy (SPE), since a high-spin ion is formed from low-spin ions. The products of Co^{3+} charge disproportionation have four unpaired d elec-

trons while the reactants have none, making the products more favorable in terms of SPE (Figure 7).

7. Summary of Important Factors Influencing Co and Mn Site Preference in ccp Oxides

The association shown in sections 4 and 5 between the +2 oxidation state and a relatively low energy for tetrahedral Mn defects in the layered structure is found to carry over to the site preference of Mn in periodic crystalline structures (likewise the high energy for Co occupancy of tetrahedral sites). Table 1 gives the calculated energy difference between layered $Li_{1/2}MO_2$ and other crystal structures with varying amounts of tetrahedral TM cations. Note that the $X_{Li} = 0.5$ structures with tetrahedral Mn in Table 1 are markedly lower in energy relative to the layered structure (l-$Li_{1/2}MO_2$) than are those with tetrahedral Co.

For the partially inverse spinel structure (ps-$(LiM)_{tet}(LiM_3)_{oct}O_8$) shown in Table 1, one-fourth of the Co or Mn in tetrahedral sites are calculated to have a +2 formal valence while three-quarters in octahedral sites adopt a +4 formal valence (giving the overall average valence of +3.5 required by charge balance). Similar to the tetrahedral defect calculations for Mn and Co at $X_{Li} = 1/2$ (Figure 4, bottom), the ps-$(LiMn)_{tet}(LiMn_3)_{oct}O_8$ is calculated to be lower in energy than l-$Li_{1/2}MnO_2$ while ps-$(LiCo)_{tet}$-$(LiCo_3)_{oct}O_8$ is calculated higher in energy than l-$Li_{1/2}$-CoO_2. The generally low energy associated with the charge disproportionation of Mn^{3+} to produce Mn_{tet}^{2+} (eq 1) indicated by the calculations of this section, as well as in sections 4 and 5, is consistent with the experimental observation that Mn^{3+} in many environments favors charge disproportionation.[52]

The importance of electron supply in the energetics of tetrahedral Mn is demonstrated by the inverse spinel (is-$(Mn_2)_{tet}(Li_2Mn_2)_{oct}O_8$) result in Table 1. In is-$(Mn_2)_{tet}(Li_2Mn_2)_{oct}O_8$ one-half of all the Mn are in tetrahedral coordination but there are not enough electrons available for these Mn to take on a +2 oxidation state without the other Mn being oxidized above +4. Instead, the valences for Mn are calculated to be +3 in tetrahedral coordination and +4 in octahedral coordination (giving the required average valence of +3.5). The relatively high energy of is-$(Mn_2)_{tet}(Li_2Mn_2)_{oct}O_8$ compared to l-$Li_{1/2}MnO_2$ further demonstrates that only the +2 oxidation state (out of the oxidation states +2 through +4) seems to be correlated with the low-energy occupation of tetrahedral sites by Mn.

Table 1. Energy of Mn and Co Oxides with Varying Amounts of Tetrahedral TM Ions (Comparison of Co and Mn oxides at $X_{Li} = 0.5$)[a]

structure	fraction of M tet	energy (eV)/M cation: $Li_{1/2}$-MnO_2	energy (eV)/M cation: $Li_{1/2}$-CoO_2
l-$Li_{1/2}MO_2$ (layered)	0	0.0	0.0
s-LiM_2O_4 (spinel)	0	−0.2489	−0.1791
$(LiM)_{tet}(LiM_3)_{oct}O_8$ (part. inv. spin.)	1/4	−0.0829	0.1448
$(M_2)_{tet}(Li_2M_2)_{oct}O_8$(inv. spin.)	1/2	0.2447	0.3627

[a] Energies are relative to the l-$Li_{1/2}MO_2$ structure for M ≡ Mn and M ≡ Co, respectively. The second column lists the fraction of TM cations in tetrahedral coordination for a given structure. The structure labeled $(LiM)_{tet}(LiM_3)_{oct}O_8$ (part. inv. spin.) corresponds to a partially inverse spinel and $(M_2)_{tet}$-$(Li_2M_2)_{oct}O_8$ (inv. spin.) to a fully inverse spinel (i.e., antispinel).

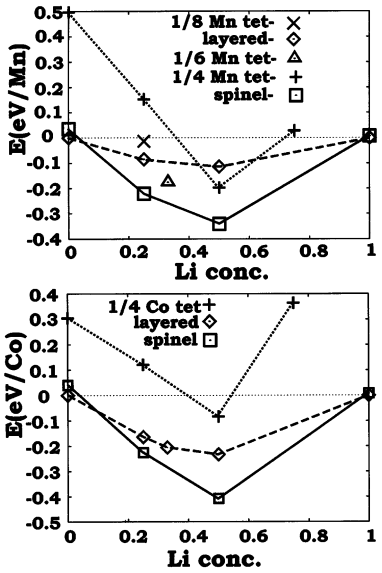

Figure 8. Formation energy versus Li concentration for three structures of Mn oxide (top) and Co oxide (bottom): (□) s-$Li_xM_2O_4$-labeled spinel, (◇) l-Li_xMnO_2-labeled layered, and (+) partially inverse spinel structure with 1/4M tetrahedral (ps-$(Li_xM)_{tet}(Li_yM_3)_{oct}O_8$; $0 \le x \le 1$ and $0 \le y \le 2$) labeled 1/4 Mn tet. As the Li content is increased, the Li is added to the tetrahedral site first of ps-$(Li_xM)_{tet}$-$(Li_yM_3)_{oct}O_8$, and then to the octahedral sites. For Mn, there also is the energy of (△) a structure with one-sixth of the Mn in tetrahedral sites at $X_{Li} = 1/3$ labeled 1/6 Mn tet with a triangle data point and (×) a structure with one-eighth of the Mn in tetrahedral sites at $X_{Li} = 1/4$ labeled 1/8 Mn tet.

Hence, the passage of Mn between octahedral sites via an intermediate tetrahedral site (i.e., the "open" $O_h \rightarrow T_d \rightarrow O_h$ path of Figure 2) is expected to be greatly facilitated when the Mn can take on a +2 valence in the tetrahedral site. The amount of Mn ions that can become +2 is determined by the average degree of Mn oxidation which is determined by the Li content.

The average Li content also determines the number of available tetrahedral sites that Mn can enter without sharing faces with Li ions in n.n. octahedral sites. Therefore, while $LiMnO_2$ has sufficient electrons available for one-half of the Mn to take on a +2 valence through charge disproportionation of Mn^{3+} (eq 1), Mn movement into tetrahedral sites in l-$LiMnO_2$ is still expected to be highly unfavorable due to electrostatic interactions with Li in face-sharing n.n. octahedra.

This interplay between electron supply and cation repulsion on the energetics of structures with tetrahedral Mn or Co is illustrated by Figure 8, which gives the calculated energies per TM ion for various structures over a range of Li contents. The results for the ps-$(Li_xM)_{tet}(Li_yM_3)_{oct}O_8$ structure ($0 \le x \le 1$ and $0 \le y \le 2$) are shown for both M ≡ Co and Mn (with increasing lithiation the Li was added to the tetrahedral sites first, then octahedral). These ener-

gies, labeled 1/4 M tet with + data points in Figure 8, are compared with the energies of the *l*-Li_xMO_2 and *s*-LiM_2O_4 structures (labeled layered with diamond data points and spinel with square data points, respectively). Additionally, for Mn the results are shown for a structure with one-sixth of the Mn in tetrahedral sites at $X_{Li} = 1/3$ (labeled 1/6 Mn tet with a triangle data point) and a structure with one-eighth of the Mn in tetrahedral sites at $X_{Li} = 1/4$ (1/8 Mn tet with a × data point). These respective Li contents were chosen because they allow the Mn to disproportionate so that all of the tetrahedral Mn are +2 and all of the octahedral Mn are +4.

When the average formal valence is +4, the calculated energy difference between *ps*-$(Mn)_{tet}(Mn_3)_{oct}O_8$ and *l*-MnO_2 is larger than that between *ps*-$(Co)_{tet}(Co_3)_{oct}O_8$ and *l*-CoO_2. This resembles the results of the tetrahedral defect calculations in *l*-MO_2 (Figure 4, top) where the energy of the tetrahedral Mn^{4+} defect is calculated to be higher than the energy of the Co_{tet}^{4+} defect.

Figure 8 shows that with the addition of Li the energy of *ps*-$(Li_xM)_{tet}(Li_yM_3)_{oct}O_8$ drops much more rapidly relative to the layered structure for Mn than for Co. Around the $Li_{1/2}MnO_2$ composition (i.e., *ps*-$(LiM)_{tet}(LiM_3)_{oct}O_8$), when all of the tetrahedral Mn have a +2 valence and all of the octahedral Mn are +4 (i.e., total charge disproportionation), *ps*-$(Li_xMn)_{tet}(Li_yMn_3)_{oct}O_8$ drops below *l*-$Li_{1/2}MnO_2$ in energy. The particularly steep drop in energy of *ps*-$(Li_xMn)_{tet}(Li_yMn_3)_{oct}O_8$ compared to *l*-Li_xMnO_2 with increasing Li concentration is due to the increase in electron supply, making more Mn_{tet}^{2+} possible.

For Co, the energy of *ps*-$(Li_xCo)_{tet}(Li_yCo_3)_{oct}O_8$ by contrast never drops below that of *l*-Li_xCoO_2. The results of Figure 8 for crystalline structures, like those in Table 1, mimic the results of the tetrahedral defect calculations (Figure 4). In each case tetrahedral Co is found to be unfavorable at all lithium concentrations and oxidation states considered, while tetrahedral Mn is found to be favorable at the $Li_{1/2}MnO_2$ composition when it has a +2 valence.

Further bolstering the association of +2 valence with low-energy tetrahedral site occupancy by Mn is the relatively low energy of Li_xMnO_2 structures with one-sixth and one-eighth of the Mn in tetrahedral coordination (marked with an × and a triangle in Figure 8) at lithium concentrations giving the tetrahedral Mn a +2 valence and the octahedral Mn a +4 valence ($Li_{1/3}MnO_2$ and $Li_{1/4}MnO_2$ compositions, respectively).

For Li concentration higher than $Li_{1/2}MO_2$ there is a rapid rise in energy for both *ps*-$(Li_xMn)_{tet}(Li_yMn_3)_{oct}O_8$ and *ps*-$(Li_xCo)_{tet}(Li_yCo_3)_{oct}O_8$ even though the tetrahedral TM ions maintain a +2 valence. The cause of this energy rise is the strong repulsion between Li^+_{oct} and Mn_{tet}^{2+} or Co_{tet}^{2+} that share a polyhedral face. Above a Li content of one-half Li per TM ion, the *ps*-$(Li_xM)_{tet}(Li_yM_3)_{oct}O_8$ structure can only accommodate Li in sites that share at least one face with another cation. At the $LiMO_2$ composition both *ps*-$(LiMn)_{tet}(Li_3Mn_3)_{oct}O_8$ and *ps*-$(LiCo)_{tet}(Li_3Co_3)_{oct}O_8$ are unstable with the tetrahedral Mn and Co being forced back into the TM layer octahedra by repulsive interactions with face-sharing Li ions (hence the lack of a + data point at $X_{Li} = 1$ in Figure 8).

Figure 8 exemplifies the conflicting requirements for low-energy occupancy and passage through tetrahedral sites by Mn in Li_xMnO_2 with a ccp oxide framework. It requires the coexistence of both Li vacancies to provide tetrahedral sites without face-sharing cations and Mn^{3+} that can form Mn_{tet}^{2+} through charge disproportionation (eq 1). However, an increase in the concentration of Li vacancies decreases the amount of Mn^{3+} that can undergo charge disproportionation (eq 1) and vice versa. This suggests that the bulk of the Mn migration out of the transition-metal layer during the transformation of *l*-Li_xMnO_2 occurs at partial lithiation when Mn^{3+} and Li vacancies coexist.[39]

The required coexistence of Mn_{oct}^{3+} and Li vacancies for the easy migration of Mn between octahedral sites via a tetrahedral intermediate also explains the ability of *s*-$Li_xMn_2O_4$ to withstand electrochemical cycling over the $0 \le X_{Li} \le 2$ range without significant cation rearrangement, even though the spinel ordering is thermodynamically unstable near $x = 0$ and 2.

When the spinel-like structure becomes metastable near $X_{Li} = 0$, most of the Mn are +4 and there are little or no Mn^{3+} that can charge disproportionate. Hence, Mn passage through tetrahedral sites is probably very unfavorable energetically. This cuts off the "open" $O_h \rightarrow T_d \rightarrow O_h$ path of Figure 2. As a result, the Mn are "trapped" in the metastable spinel-like configuration (λ-MnO2) at high charge. When the spinel structure becomes metastable near $X_{Li} = 2$ there is a lack of Li vacancies. This also prevents Mn rearrangement even though Mn_{oct}^{3+}, which can undergo charge disproportionation, are in abundance. Consequently, the metastable *s*-$Li_2Mn_2O_4$ is preserved at deep discharge as well. When Mn_{oct}^{3+}, which can charge disproportionate, and Li vacancies coexist at one-half lithiation, the spinel structure is thermodynamically stable. Therefore, when the Mn are most prone to migration, there is no thermodynamic driving force to do so and the spinel host structure is retained (although Mn can still dissolve into the electrolyte through charge disproportionation).

This discussion has focused on stoichiometric spinel structure, but nonstoichiometric spinels can exist as well. In the case of spinels that are oxygen deficient there could be significant concentrations of Mn^{3+} remaining at full charge. The results of this study suggest that such spinels may be susceptible to cation rearrangement if they are energetically metastable.

8. Effect of Chemical Substitutions on Mn Site Preference

In sections 4, 5, and 7 it was shown how low-energy occupation and passage through tetrahedral sites by Mn is associated with the +2 oxidation state. It was also shown that Mn_{oct}^{3+} can readily produce Mn_{tet}^{2+} through charge disproportionation (eq 1). On the other hand, tetrahedral Mn with a +3 or +4 oxidation state was found to be less favorable.

Chemical substitutions that oxidize Mn_{oct}^{3+}, which might otherwise produce Mn_{tet}^{2+} through charge

disproportionation, are a promising approach for hindering the transformation of metastable host structures such as l-Li_xMnO_2. Such chemical substitutions would be expected to hinder Mn passage along $O_h \rightarrow T_d \rightarrow O_h$ (Figure 2) type paths.

There are two categories of elements that will likely produce the desired effect: fixed low-valence cations and electronegative (relative to Mn_{oct}^{3+}) multivalent cations. It should be noted that fixed low-valence cations have the drawback of reducing the capacity since it is extremely difficult to oxidize Mn above +4. Some cations in these categories that have already been shown experimentally to improve the electrochemical performance of l-Li_xMnO_2 and/or o-Li_xMnO_2 include Al^{3+},[18] Co^{3+},[7] Cr^{3+},[53] Ni^{2+},[54] Li^+, and Cr^{3+}.[55]

A series of first-principles results will now be shown that demonstrate the effect of a variety of chemical substitutions on the valence of Mn and how this in turn affects the site preference of Mn.

As discussed previously, a strong preference by Mn for octahedral over tetrahedral coordination should result in reduced mobility for Mn through a ccp oxygen framework. A reduced mobility for Mn in turn could increase the resistance of metastable chemically substituted Mn oxide structures against structural transformation.

The results of sections 4, 5, and 7 indicate that there is a good correlation between the energetics of a tetrahedral Mn defect in l-Li_xMnO_2 and the energy difference between l-Li_xMnO_2 and a periodic small unit cell structure with tetrahedral Mn like ps-$(Li_xMn)_{tet}(Li_yMn_3)_{oct}O_8$ provided the Li contents and tetrahedral Mn oxidation states are the same in both the periodic structure and the tetrahedral Mn defect calculation. Specifically, Mn_{tet}^{4+} is found to be relatively unfavorable whether it occurs as a defect in layered l-MnO_2 or within a periodic structure like ps-$(Mn)_{tet}(Mn_3)_{oct}O_8$. Likewise, Mn_{tet}^{2+} is found to be relatively favorable whether it occurs as a defect in layered l-$Li_{1/2}MnO_2$ or within ps-$(LiMn)_{tet}(LiMn_3)_{oct}O_8$.

To gauge the favorability of Mn entering tetrahedral sites in the presence of chemical substitutions that alter the Mn oxidation state, the energy difference between structures such as ps-$(LiMn)_{tet}(Li\mathit{Sub}_3)_{oct}O_8$ ($\mathit{Sub} \equiv$ Mn and/or substitutional elements) with tetrahedral Mn and l-$Li_{1/2}Mn_{1/4}\mathit{Sub}_{3/4}O_2$ ($\mathit{Sub} \equiv$ Mn and/or substitutional elements) without tetrahedral Mn have been evaluated over a large range of chemical substitutions.

It is assumed that as with pure Mn oxides, the site preference for Mn at a given valence will be reflected by the energy difference between the chemically substituted compounds with and without tetrahedral Mn. The use of simple structures such as ps-$(LiMn)_{tet}$-$(Li\mathit{Sub}_3)_{oct}O_8$ with tetrahedral Mn instead of large supercells with tetrahedral Mn defects, like those used in section 4, greatly reduces the calculation time.

Obviously it is an approximation to use the energy difference between a structure with tetrahedral Mn and a structure with only octahedral Mn as an indication of Mn mobility in a ccp oxide. To precisely determine Mn mobility along the "open" $O_h \rightarrow T_d \rightarrow O_h$ path, the activation barrier is the required quantity not the energy in tetrahedral coordination. However, if the energy of tetrahedral site occupancy for Mn is high, the activation barrier for the $O_h \rightarrow T_d \rightarrow O_h$ path can only be equal or higher. Therefore, the energetics of Mn in tetrahedral coordination can provide an upper bound on the mobility of Mn along the $O_h \rightarrow T_d \rightarrow O_h$ path.

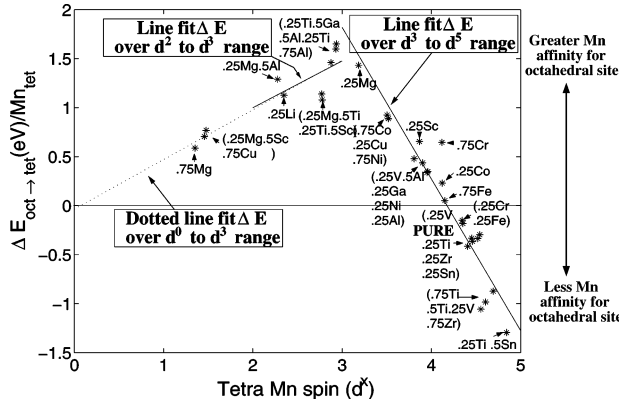

Figure 9. Energy difference between ps-$(LiMn)_{tet}(Li\mathit{Sub}_3)_{oct}O_8$ with tetrahedral Mn and l-$Li_{1/2}Mn_{1/4}\mathit{Sub}_{3/4}O_2$ without tetrahedral Mn as a function of the spin on the tetrahedral Mn (Tetra Mn spin d^x). $\mathit{Sub} \equiv$ elements substituted for Mn and/or Mn. Pure $Li_{1/2}MnO_2$ is labeled "pure". Each data point (*) has been labeled according to the element substituted (e.g., Co) and the fraction of Mn in the "pure" structural counterpart they have replaced (e.g., 0.25). The substituted elements occupy only O_h sites in both ps-$(LiMn)_{tet}(Li\mathit{Sub}_3)_{oct}O_8$ and l-$Li_{1/2}Mn_{1/4}\mathit{Sub}_{3/4}O_2$. Mn occupies T_d sites and any available O_h sites in ps-$(LiMn)_{tet}(Li\mathit{Sub}_3)_{oct}O_8$ and only O_h sites in l-$Li_{1/2}Mn_{1/4}\mathit{Sub}_{3/4}O_2$. For data points that are clumped together, a single label containing all the chemical substitutions contained in the cluster of points is enclosed in parentheses (e.g., 0.25Cr, 0.25Fe). The chemical substitutions listed in these labels are ordered (going from top to bottom in the label) from lowest Mn_{tet} d spin to highest, i.e., from left-most data point to right-most in the cluster. The data points for 0.25 Cu and 0.75 Ni cannot be resolved because they have nearly the same coordinates: (0.25 Cu, 3.517, 0.887 eV); (0.75 Ni, 3.519, 0.886 eV).

Figure 9 shows the energy difference between ps-$(LiMn)_{tet}(Li\mathit{Sub}_3)_{oct}O_8$ ($\mathit{Sub} \equiv$ Mn and/or elements substituted for Mn) and l-$Li_{1/2}Mn_{1/4}\mathit{Sub}_{3/4}O_2$, which is believed to be a particularly good gauge for the stability of the layered structure. The reason for this is that ps-$(LiMn)_{tet}(Li\mathit{Sub}_3)_{oct}O_8$ is equivalent to a tetrahedral Mn and Li defect placed in a small supercell of layered structure (four MnO_2 units as opposed to the 12 and 32 MnO_2 unit supercells used in section 4). Hence, its energy should be related to the Mn tetrahedral defect energy in layered at a given composition. Furthermore, the partially inverse spinel (ps-$(LiMn)_{tet}(Li\mathit{Sub}_3)_{oct}O_8$) can be easily formed from l-$Li_{1/2}Mn_{1/4}\mathit{Sub}_{3/4}O_2$ by moving one-fourth of the Mn into nearest neighbor tetrahedra in the Li layer, which equals the fraction of Mn that move from the TM layer to the Li layer during the transformation of layered to spinel (i.e., one Mn per eight oxygen).[78,79] Therefore, ps-$(LiMn)_{tet}(Li\mathit{Sub}_3)_{oct}O_8$ could resemble intermediate structures that arise during the transformation.

Consistent with the proposed importance of Mn valence and LFSE, low fixed valence cations (e.g., Al^{3+}, Mg^{2+}, Li^+) and electronegative multivalent

cations (e.g., Co^{3+}, Ni^{2+}, Cu^{2+}) that oxidize Mn^{3+} are calculated to stabilize Mn in the octahedral sites of l-$Li_{1/2}Mn_{1/4}Sub_{3/4}O_2$. This is indicated in Figure 9 by the ps-$(LiMn)_{tet}(LiSub_3)_{oct}O_8$ with these chemical substitutions (i.e., $Sub \equiv$ Al, Mg, Li, Co, Ni, or Cu) being higher in energy than l-$Li_{1/2}Mn_{1/4}Sub_{3/4}O_2$ rather than lower as is the case for pure $Li_{1/2}MnO_2$ (labeled "pure" in Figure 9).

The correspondence between chemical substitutions that have been reported to experimentally stabilize layered l-Li_xMnO_2 material and/or improve its capacity (e.g., Al^{3+}, Co^{3+}, Cr^{3+}, Ni^{2+}, Li^+) and the chemical substitutions that are calculated to stabilize Mn in the layered octahedral sites according to Figure 9 is reassuring.[7,18,53−55] Another encouraging feature of Figure 9 is that none of the elements that are found in compositions calculated to destabilize the layered structure (e.g., Ti^{4+}, Zr^{4+}, Sn^{4+}, V^{5+}) have been reported experimentally to be successful in stabilizing l-Li_xMnO_2 material.

Cr substitution provides a particular example that supports interpreting the results of Figure 9 as a measure of the layered structures stability against transformation. Experiments have shown that reducing the Mn/Cr ratio in Cr-substituted l-Li_xMnO_2 reduces in size or eliminates the spinel-type step in the voltage curve that arises during electrochemical cycling of pure l-Li_xMnO_2.[53,56] This implies that Cr substitution can hinder or prevent the transformation of the layered structure to spinel.

Davidson et al. found that replacing one-fourth of the Mn in l-Li_xMnO_2 with Cr fails to prevent a step in the voltage curve from developing with electrochemical cycling.[53] The calculated energy of the partially inverse spinel (ps-$(LiMn)_{tet}(LiCrMn_2)_{oct}O_8$) with one-fourth of the Mn substituted with Cr is −0.1494 eV/(Mn_{tet}) lower in energy than l-$Li_{1/2}(Cr_{1/4}Mn_{3/4})O_2$. Using this result as a gauge of stability suggests that the layered structure with one-fourth Cr should still be susceptible to forming tetrahedral Mn and hence should still be susceptible to transforming into spinel, consistent with experimental observation.

A compound with one-half of the Mn ions substituted by Cr was found to have no spinel step in its voltage curve.[53] The energy of $(LiMn)_{tet}(LiCr_2Mn)_{oct}O_8$ for this case is calculated to be 0.2806 eV/(Mn_{tet}) higher in energy than l-$Li_{1/2}(Cr_{1/2}Mn_{1/2})O_2$.[24] This result suggests that forming tetrahedral Mn in the layered structure with one-half Cr should be unfavorable, and hence the structure should resist transforming into spinel, again consistent with observation. While Figure 9 may give a measure of the stability of chemically substituted layered compounds against Mn migration into the Li/vacancy layer, it should be kept in mind that the elements substituted for Mn may themselves be prone to migration into the Li/vacancy layer. However, in the Davidson experiment it appears that both the Cr and Mn resist migrating into the Li/vacancy layer when the Mn is sufficiently oxidized.

In addition to revealing which chemical substitutions could prevent the transformation of the layer structure, Figure 9 also illustrates the relation

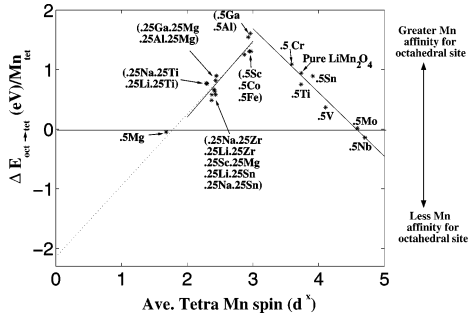

Figure 10. Equivalent plot to Figure 9 except ΔE gives the energy difference between fully inverse spinel, i.e., antispinel (is-$Mn_{tet}(LiSub)_{oct}O_4$; $Sub \equiv$ substitutional elements or Mn) and spinel (s-$Li_{tet}(MnSub)_{oct}O_4$). Also, the x axis is now the average spin on the tetrahedral Mn since there are two tetrahedral Mn per inverse spinel unit cell. All of the chemical substitutions replace 50% of the Mn ions. In the anti-spinel, all of the octahedral Mn are chemically substituted. In the spinel half of the octahedral Mn are chemically substituted.

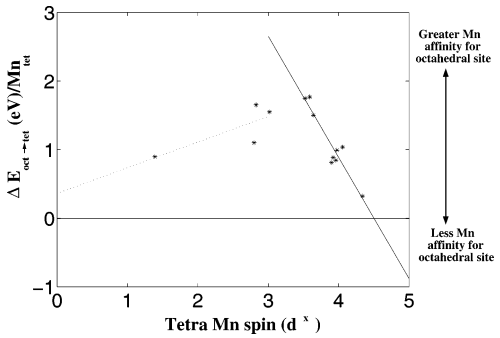

Figure 11. Equivalent plot to Figure 9 at $X_{Li} = 0.25$.

between the valence of Mn and its energy in tetrahedral coordination. Starting at Mn_{tet}^{2+} (i.e., d^5 filling), the relative energy of ps-$(LiMn)_{tet}(LiSub_3)_{oct}O_8$ rises roughly linearly with increasing valence (i.e., decreasing d filling) to a maximum peak at around +4 valence (i.e., d^3 filling) for the tetrahedral Mn.

This is consistent with calculations shown in sections 4, 5, and 7 that found the tetrahedral Mn^{4+} defect (Figure 4) as well as the delithiated ps-$(Mn)_{tet}(Mn_3)_{oct}O_8$ (Figure 8) to be particularly high in energy. It is also consistent with experimental results that show chemical substitutions which oxidize Mn to +4 such as Ni[40] increase the stability of the layered structure.[54] When Mn is oxidized to +4 it becomes, practically speaking, electrochemically inactive in l-Li_xMO_2 materials due to the great difficultly in oxidizing Mn above +4.

Figure 9 indicates that chemical substitutions which oxidize Mn stabilize the layered structure against transformation only up to a point. At valences higher than +4, i.e., tetrahedral Mn orbital fillings less than d^3, the trend abruptly shifts (Figure 9). Although in reality such valences are rare for Mn in ccp oxides, Mn is predicted to become less stable in the layered octahedral sites with valences increasing above +4.

Figures 10−13 give further confirmation that the maximum energy for Mn occupation of tetrahedral sites in a ccp oxide occurs when the Mn valence is +4 (i.e., d^3 filling), independent of cation ordering. Figures

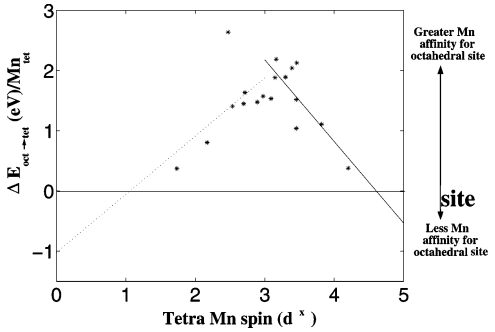

Figure 12. Equivalent plot to Figure 9 at $X_{Li} = 0$.

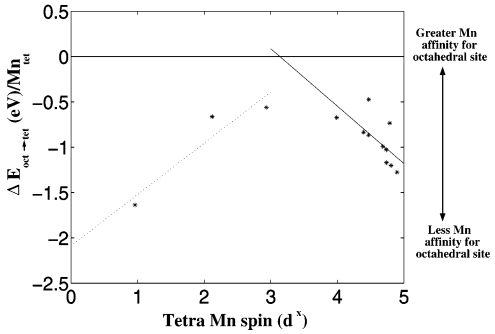

Figure 13. Energy difference between the *s*-$(Mn)_{tet}$-$(Sub_2)_{oct}O_4$ spinel and *rs*-$(MnSub_2)_{oct}O_4$ cation-deficient rock-salt structures.

10−13 contain energy plots equivalent to Figure 9 that were generated from comparisons between fully inverse spinel (*is*-$(Mn)_{tet}(LiSub)_{oct}O_4$) and spinel (*s*-$Li(MnSub)O_4$), *ps*-$(LiMn)_{tet}(Sub_3)_{oct}O_8$ and *l*-$Li_{1/4}Mn_{1/4}Sub_{3/4}O_2$, *ps*-$(Mn)_{tet}(Sub_3)_{oct}O_8$ and *l*-$Mn_{1/4}Sub_{3/4}O_2$, spinel *s*-$(Mn)_{tet}(Sub_2)_{oct}O_4$ and cation-deficient rock-salt *rs*-$(MnSub_2)_{oct}O_4$. Figure 10 is particularly notable because it illustrates how chemical substitutions which reduce Mn_{tet} toward an ideal +2 d-orbital filling (e.g., 0.5 Nb), or that oxidize Mn_{tet} well above +4 (e.g., 0.5 Mg) are calculated to actually make the fully inverse spinel with tetrahedral Mn more stable than spinel at one-half lithiation.

8.1. Electronic Structure Model for the Energetics of Mn Oxides

Figures 9−13 show that the energy difference between structures with and without tetrahedral Mn is approximately a linear function of d-orbital filling on the tetrahedral Mn within certain ranges.

One can intuitively understand the piecewise linear structure of the plots in Figures 9−13 using a simple model based on the change in electronic structure when Mn moves from an octahedral to a tetrahedral site. In this model it is assumed that the slopes of the lines in Figures 9−13 are equal to the energy difference between the energetically highest occupied d orbital (HODO) of the tetrahedral Mn and the HODO of the octahedral Mn. This assumption is consistent with electrons being transferred between octahedral d levels and tetrahedral d levels that are fixed with respect to each other independent of oxidation state.

Given the typical d-orbital splitting for tetrahedral and octahedral environments this leads to three different regimes for the energy change when Mn moves from octahedral to tetrahedral coordination as illustrated in Figure 14 (this model neglects the splitting of the e_g level by Jahn−Teller distortion). Figure 14 schematically pictures how the d orbitals change for a Mn that moves from octahedral (O_h) coordination (e.g., in the layered structure) to tetrahedral (T_d) coordination (e.g., tetrahedral site in *ps*-$(LiMn)_{tet}(LiSub_3)_{oct}O_8$).

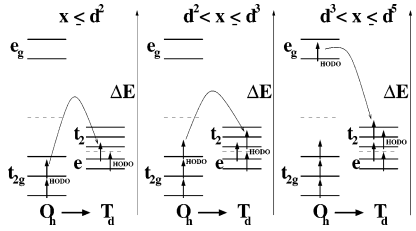

Figure 14. In tetrahedral coordination (T_d) the d-orbital splitting is opposite and smaller in magnitude than the d-orbital splitting in octahedral coordination (O_h). Consequently, the transfer of electrons from d orbitals in an O_h ligand field to d orbitals in a T_d field as Mn moves from an octahedral to a tetrahedral site falls into three different regimes: $x \leq 2$, $2 < x \leq 3$, and $3 < x \leq 5$. These regimes are distinguished by the highest occupied d orbital (HODO) in the O_h and T_d fields. Only integer fillings of the d shell are pictured, but fractional fillings can occur as well.

The different regimes that occur as a function of the tetrahedral Mn d-orbital filling (d^x) are as follows.

(1) $x \leq 2$. In this regime as Mn moves from octahedral to tetrahedral coordination the d electrons move from t_{2g} (lowered octahedral d) to e (lowered tetrahedral d) orbitals. The energy difference between tetrahedral and octahedral Mn is given by the energy difference between the filled e and t_{2g} orbitals plus a constant ($\Delta E_{Mn^{7+}}$) that accounts for other energy contributions independent of d-orbital filling ($\Delta E_{Mn^{7+}}$ is the ΔE intercept at d^0 of Figures 9−13).

$$\Delta E_{oct \rightarrow tet} = (E_e - E_{t_{2g}})x + \Delta E_{Mn^{7+}} \quad (3)$$

(2) $2 < x \leq 3$. The energy difference in this regime includes the contribution from the $x \leq 2$ regime plus the energy difference between the filled t_2 (raised tetrahedral d) and the t_{2g} (lowered octahedral d) orbitals giving

$$\Delta E_{oct \rightarrow tet} = (E_{t_2} - E_{t_{2g}})(x - 2) + 2(E_e - E_{t_{2g}}) + \Delta E_{Mn^{7+}} \quad (4)$$

(3) $3 < x \leq 5$. The energy difference in this regime includes the contribution from the $x \leq 2$ and $2 < x \leq 3$ regimes plus the energy difference between the filled t_2 (raised tetrahedral d) and e_g (raised octahedral d) orbitals giving

$$\Delta E_{oct \rightarrow tet} = (E_{t_2} - E_{e_g})(x - 3) + (E_{t_2} - E_{t_{2g}}) + 2(E_e - E_{t_{2g}}) + \Delta E_{Mn^{7+}} \quad (5)$$

This simple model, which gives a piecewise linear relationship between the energy of tetrahedral Mn and its valence, fits the results of Figures 9−13 surprisingly well, considering the wide variety of single and multivalent cation substitutions used in generating these plots. This again indicates the

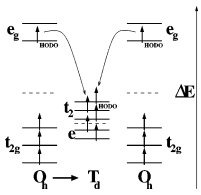

Figure 15. Schematic of the charge disproportionation reaction which involves two Mn as opposed to the single Mn reactions shown in Figure 14. Charge disproportionation can occur over the $3 < x \leq 5$ filling range. The set of orbitals O_h and T_d linked by a right arrow (→) correspond to the Mn moving from octahedral to tetrahedral coordination. The other set of orbitals labeled O_h correspond to a Mn that remains in octahedral coordination. Integer fillings of the d shell are pictured, but fractional fillings can occur as well.

substantial role Mn valence plays in determining its site energy.

The model of eqs 3−5 suggests that the energy of a manganese oxide can be conveniently separated into two contributions. One contribution is from the interactions involving Li cations, O anions, Mn^{7+} (i.e., d^0) ionic cores, and elements substituting for Mn (d^0 ionic cores if the d orbitals of these elements are filled). The difference in this energy term between the structures with and without tetrahedral Mn equals the *y* intercept ($\Delta E_{Mn^{7+}}$) of $\Delta E_{oct \rightarrow tet}$ given by eqs 3−5. The other energy contribution is from the energy of the filled Mn d orbitals (and in some instances the substitutional element d orbitals) which gives the piecewise linear valence dependent terms of $\Delta E_{oct \rightarrow tet}$ in eqs 3−5.

The simple d-level splitting model of eqs 3−5 explains well the abrupt change in slope as the orbital filling moves from the $2 < x \leq 3$ regime to the $3 < x \leq 5$ regime (Figures 9−12). When the filling of the Mn d orbitals exceeds d^3, the HODO of the octahedral Mn goes from being lower in energy (t_{2g}) to higher in energy (e_g) than the HODO of the tetrahedral Mn (t_2). Therefore, at d^3 the slope of $\Delta E_{oct \rightarrow tet}$ as a function of Mn_{tet} d filling abruptly changes sign from positive to negative. The $x \leq 2$ regime cannot be resolved from the $2 < x \leq 3$ regime in Figures 9−13, which suggests that there is little splitting between the Mn d orbitals in tetrahedral coordination (i.e., t_2 and e).

While Figure 14 only illustrates a single Mn^{7+} ion core and its associated d electrons moving from O_h to T_d coordination, the proposed model of eqs 3−5 can also be used to account for charge disproportionation (eq 1). When charge disproportionation occurs an additional electron is transferred to the tetrahedral Mn t_2 orbital from a Mn e_g orbital (or perhaps another multivalent cation d orbital) that remains in octahedral coordination. The HODOs over the $3 < x \leq 5$ d-filling regime (i.e., t_2 tetrahedral, e_g octahedral) remain the same whether charge disproportionation occurs or not. Therefore, the presence of charge disproportionation should not change the slope of the plot over the $3 < x \leq 5$ regime according to eq 5. This can be seen by comparing the $3 < x \leq 5$ regime of Figure 14 with the disproportionation reaction diagramed in Figure 15.

Equations 3−5 can be used to estimate the octahedral ligand-field splitting (Δ_o) from the slopes of the lines fit to Figures 9−13. The octahedral ligand-field splitting is found to be roughly the same for all of the MnO_2 host structures and Li contents considered (i.e., Figures 9−12), ranging from $\Delta_o = 2.1$ to 2.3 eV. These values resemble the ligand-field splitting reported experimentally for MnO_2 of 2.5 eV.[57] The estimated octahedral ligand-field splitting for the Mn_3O_4 structures on the other hand (Figure 13) is found to much lower at $\Delta_o = 1.2$ eV. This is close to the ligand-field splitting reported experimentally for MnO of 1.3 eV.[57]

In addition to having a lower estimated Δ_o, the calculations on Mn_3O_4 (Figure 13) differ from the MnO_2 host structures in having the *y* intercept $\Delta E_{Mn^{7+}}$ shifted to such a negative value that the tetrahedral Mn structure (s-$(Mn)_{tet}(Sub_2)_{oct}O_4$) is always lower in energy than the structure with only octahedral Mn (rs-$(MnSub_2)_{oct}O_4$), although a maximum in energy at Mn_{tet}^{4+} is maintained.

While the piecewise linear regions and energy maximum around +4 valence of Figures 9−13 are consistent with ligand-field effects, it is important to bear in mind that LFSE cannot by itself predict the energy difference between octahedral and tetrahedral Mn.

For example, in section 6 the change in LFSE associated with the charge disproportionation reaction creating tetrahedral Mn^{2+} (eq 1) is projected to be equal to the Jahn−Teller splitting α, i.e., a positive energy (see Figure 7). However, first-principles calculations show that the energy of producing tetrahedral Mn^{2+} through charge disproportionation (eq 1) in l-$Li_{1/2}MnO_2$ is negative (Figures 4, 8, and 9).

The possibility that Mn generally favors tetrahedral coordination as its valence approaches +2 (i.e., d^5) is unlikely given that MnO has a rock-salt structure not zinc blende or some other structure with Mn_{tet}^{2+}. Instead, the driving force for Mn movement out of the octahedral sites of l-$Li_{1/2}MnO_2$ into neighboring Li layer tetrahedral sites appears to be due to the unique cationic ordering and associated cationic interactions that are present in l-$Li_{1/2}MnO_2$.

In the case of l-$Li_{1/2}MnO_2$, the positive change in LFSE for charge disproportionation (i.e., α) is insufficient to counter the cationic interactions that favor Mn movement into Li layer tetrahedra. Conversely, in chemically substituted compounds such as l-$Li_{1/2}Mn_{3/4}Mg_{1/4}O_2$, the much higher change in LFSE associated with Mn^{4+} movement from octahedral to tetrahedral coordination ($38/45\ \Delta_o$ assuming $-4/9\Delta_o = \Delta_t$) overwhelms the interactions favoring the formation of tetrahedral Mn^{4+} so that it becomes highly unfavorable energetically.

While LFSE can be useful for explaining the trends of Mn site preference with valence, it does not capture important energy contributions that are more sensitive to cationic ordering. These energy contributions, for example, make the formation of tetrahedral Mn^{2+} favorable in l-$Li_{1/2}MnO_2$ but unfavorable in s-$LiMn_2O_4$. A more clear picture of these energy contributions can be gained from the model of eqs 3−5.

One energy contribution that is sensitive to cationic ordering given explicitly in eqs 3−5 is the y intercept $\Delta E_{Mn^{7+}}$. According to the proposed model $\Delta E_{Mn^{7+}}$

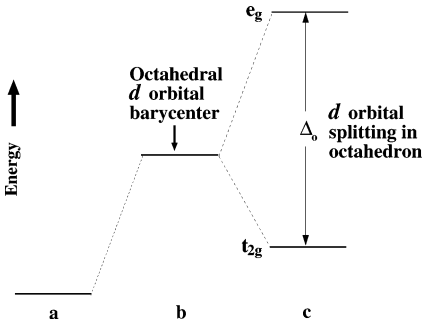

Figure 16. Effect of octahedral coordination on the energy of TM 3d orbitals: (a) 3d level of free TM ion. 3d orbitals are degenerate. (b) Average interactions between anions, neighboring cations, and 3d electrons shift the average energy of the 3d orbitals. (c) Splitting of 3d energy levels in an octahedral ligand field. Note that while the energy of the 3d orbitals may be increasing due to the negatively charged ligands, the overall energy of the system is decreasing in going from a free ion to bound one.

accounts for the interactions involving Li cations, O anions, Mn^{7+} (i.e., d^0) ionic cores, and elements substituting for Mn (d^0 ionic cores if the d orbitals of these elements are filled). It is assumed that these interactions are primarily electrostatic. $\Delta E_{Mn^{7+}}$ can have a substantial effect on site energetics as the difference in *y*-intercepts of Figures 9−13 show.

The other energy contribution that is sensitive to cationic ordering is implicitly part of d-orbital terms such as $(E_{t_2} - E_{e_g})(x - 3)$ in eqs 3−5. A coefficient such as $(E_{t_2} - E_{e_g})$, which gives the energy difference between the tetrahedral t_2 and octahedral e_g orbitals, can be broken down into two parts.

One part depends on the ligand-field splitting in a given coordination (i.e., Δ_o and Δ_t). This part is the change in LFSE is represented in Figure 7 (e.g., α for Mn charge disproportionation; eq 1, 38/45 Δ_o for Mn^{4+} $O_h \rightarrow T_d$).

The other part depends on the average energy of the d orbitals, i.e., the energy barycenter, in a given site. The energy barycenter of d orbitals in octahedral coordination is represented by the level above b in Figure 16.[45] In moving Mn between octahedral and tetrahedral sites there is a change in LFSE caused by the change in the splitting of the d orbitals (e.g., from t_{2g} and e_g to e and t_2) and a change in energy barycenter caused by the change in the average interactions experienced by electrons in the d orbitals.

Taking into account the change in barycenter of the d levels and the interactions involving the Mn^{7+} ionic cores, a more complete expression for the energy change (ΔE_{cd}) associated with the Mn charge disproportionation reaction (eq 1) than that given in Figure 7 can be obtained

$$\Delta E_{cd} = (5E_{tb} + E_{Mn_{tet}{}^{7+}}) + \left(3E_{ob} - \frac{6}{5}\Delta_o + E_{Mn_{oct}{}^{7+}}\right) - 2\left(4E_{ob} - \frac{3}{5}\Delta_o - \frac{\alpha}{2} + E_{Mn_{oct}{}^{7+}}\right)$$

$$\Delta E_{cd} = 5(E_{tb} - E_{ob}) + \alpha + (E_{Mn_{tet}{}^{7+}} - E_{Mn_{oct}{}^{7+}})$$

$$\Delta E_{cd} = 5\Delta E_b + \alpha + \Delta E_{Mn^{7+}} \quad (6)$$

The change in LFSE of α associated with the charge disproportionation reaction of Mn (Figure 7) is now augmented with two other terms to give a more complete expression for the total energy change: ΔE_b, which equals the change in the d barycenter ($E_{tb} - E_{ob}$), and $\Delta E_{Mn^{7+}}$, which equals the change in Mn core interaction energies when Mn moves from an octahedral to a tetrahedral site ($E_{Mn_{tet}{}^{7+}} - E_{Mn_{oct}{}^{7+}}$).

Equation 6 helps clarify why the energy of the charge disproportionation reaction producing tetrahedral Mn in *l*-$Li_{1/2}MnO_2$ is negative. The *y* intercept of Figure 9 is close to zero, which indicates that $\Delta E_{Mn^{7+}} \approx 0$ when changing from *l*-$Li_{1/2}MnO_2$ to (*ps*-$(LiMn)_{tet}(LiMn_3)_{oct}O_8$). Therefore, in this case the energy of charge disproportionation is approximately $\Delta E_{cd} = 5\Delta E_b + \alpha$. Since α is positive, ΔE_b must be negative for the formation of tetrahedral Mn in *l*-$Li_{1/2}MnO_2$ to be energetically favored. In other words, the d-orbital energy barycenter in *ps*-$(LiM)_{tet}(LiM_3)_{oct}O_8$ is lower than the barycenter in *l*-$Li_{1/2}MnO_2$ according to this model.

Just as values for Δ_o can be estimated from Figures 9−13 using eqs 3−5, so to can values for ΔE_b and $\Delta E_{Mn^{7+}}$. Whereas Δ_o is estimated to be roughly constant (2.1−2.3 eV) for the MnO_2 host structures (Figures 9−12), the values of ΔE_b and $\Delta E_{Mn^{7+}}$ are estimated to vary much more widely (−0.48 to 0.29 eV and −2.1 to 0.36 eV, respectively). This is consistent with the d-orbital barycenter and the Mn^{7+} core interactions being more sensitive to cationic ordering than the ligand-field splitting, as previously suggested.

Since the LFSE term is determined by Mn valence and appears to be relatively insensitive to cation ordering in the MnO_2 host structures, it would seem to be the easiest energy term to manipulate through chemical substitutions. This is because the exact placement of the chemical substitutions in the Mn sublattice would presumably be less important for the LFSE term than for the terms that are more sensitive to cationic ordering (i.e., ΔE_b and $\Delta E_{Mn^{7+}}$).

9. Qualitative Ionization Scale

The previous sections highlighted the role valence plays in determining Mn site preference and mobility through a ccp oxide framework and consequently in the susceptibility of metastable structures such as *l*-Li_xMnO_2 to structural transformation. Since chemical substitutions are one way of manipulating the valence of Mn, it is useful to be able to predict the effect substituted cations will have on the valence of Mn in either tetrahedral or octahedral sites. The large number of calculations used to produce Figures 9−13 can be used to provide a qualitative oxidation scale between Mn and other 3d TM ions. The relative oxidation/reduction strength of the substituted TM ions that Mn coexists with in Figures 9−13 can by obtained by determining the valence of each cation using the spin integration method described in section 5.

Figure 17 holds in a compact form all of the valence information on crystalline TM oxides produced by the first-principles calculations of this study. The position of a given ion pair (e.g., $Ni_{oct}{}^{3+\rightarrow 4+}$) on the chart

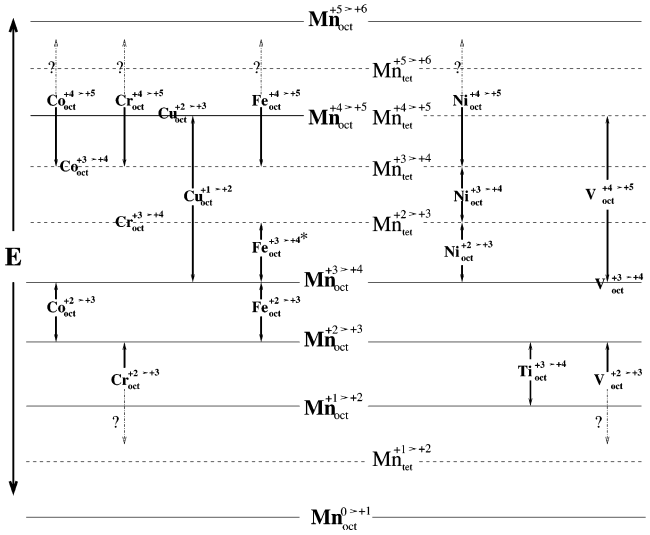

Figure 17. Qualitative ionization energies for 3d ions at various valences in an oxide framework. The position of a given ion pair indicates the energy ranking of that ionization reaction. Comparisons are relative to Mn ionization energies in O_h and T_d coordination labeled prominently in the center of the figure. Solid black arrows indicate well-determined upper and/or lower energy limits for a given ionization energy. Dashed lines with a question mark indicate that in that direction the energy limit was not determined. For example, the ionization energy $Cr_{oct}^{2+\rightarrow3+}$ is calculated to be lower in energy than $Mn_{oct}^{2+\rightarrow3+}$ but it is uncertain which Mn ionization energy it lies above. If an ionization energy lies at the same level as one of the Mn energies and does not have an arrow on either side (e.g., $Co_{oct}^{3+\rightarrow4+}$), that ionization energy and the Mn energy which it is level with were found to be approximately equal in energy (i.e., $Co_{oct}^{3+\rightarrow4+} \approx Mn_{tet}^{3+\rightarrow4+}$). The chart entry $Fe_{oct}^{3+\rightarrow4+}$ marked with an asterisk (*) contradicts the result calculated for anti-spinel $(Mn)_2(Li_2Fe_2)O_8$ but it is consistent with all other calculations performed on $Li_x(MnFe)O_2$ structures.

indicates the relative energy ranking of that ionization reaction (e.g., the ionization energy of Ni_{oct}^{3+} to Ni_{oct}^{4+}) compared to the various ionization energies of Mn in octahedral and tetrahedral coordination. The qualitative ranking of the Mn ionization energies in octahedral and tetrahedral coordination is labeled prominently along the center of Figure 17.

The purpose of this scale is to aid in qualitatively predicting the effect of 3d TM ion chemical substitutions on the valence of Mn in octahedral or tetrahedral sites of a ccp oxide. This scale can be useful for choosing chemical substitutions that will keep octahedral Mn in a relatively immobile valence state (i.e., near +4) over the range of an electrochemical cycle where the coexistence of Mn^{3+} and Li vacancies would allow the rapid transformation of a metastable ccp oxide (e.g., as with *l*-Li_xMnO_2 or *o*-Li_xMnO_2).

To illustrate the use of the qualitative ionization scale given in Figure 17, consider the case of layered $Li(Ni_{1/2}Mn_{1/2})O_2$.[58] Assuming that the oxidation states of Li and O are +1 and −2, respectively (calculated to be true except in extremely electron-deficient cases), Ni and Mn must hold an average valence of +3. Moving up from the bottom of the scale one notes $Mn_{oct}^{3+\rightarrow4+}$ is ranked lower than $Ni_{oct}^{2+\rightarrow3+}$. This means Mn^{3+} is favored to be oxidized to +4 over Ni^{2+} being oxidized to +3. Since one-half Mn^{4+} and one-half Ni^{2+} gives an average valence of +3 required by the Li content, the predicted valences are Mn^{4+} and Ni^{2+}. This matches calculated[40] and experimental results.[59]

Since Figure 17 is constructed only with calculations on Mn oxides substituted with *one* other 3d metal, it is not clear whether using Figure 17 to predict the valence of two or more non-Mn 3d TM ions coexisting in an oxide would be valid. However, with additional calculations on non-Mn TM oxide compositions perhaps Figure 17 can be expanded to address combinations of non-Mn TM ions.

10. Effect of Valence on Site Preference of Other 3d Transition Metals

Since the results of the previous sections indicate that the site preference and tendency toward migration of Mn or Co is strongly affected by the electron occupancy of the d levels split by ligand-field effects, it is possible that this may be the case for all of the 3d TM ions.

The 3d orbitals of Mn and Co and those of the other first-row transition metals should have a qualitatively similar ligand-field splitting in octahedral or tetrahedral sites of an oxide.[44,45] The magnitude of the splitting may vary as it depends on the extent of overlap between the TM d and oxygen p states.[46,60] However, as a first approximation it is instructive to neglect this variation in ligand-field splitting across the 3d series and simply characterize a TM ion at a given valence by the number and configuration (e.g., high or low spin) of its d electrons. For example, Fe^{3+} would be expected to behave somewhat similar to Mn^{2+} when both have a high-spin d^5 configuration (e.g., $t_{2g}^3e_g^2$ in octahedral coordination).

The relative energetics of tetrahedral and octahedral occupancy for Mn and Co in a ccp oxide with $Li_{1/2}MO_2$ composition was observed to be consistent with the projected change in LFSE for Mn and Co when they are moved from octahedral to tetrahedral coordination (Figure 7; section 6). To test how well this trend holds for other 3d transition metals, calculations equivalent to those done with Mn and Co in section 7 were performed for the transition metals Ti through Cu on the *ps*-$(LiM)_{tet}(LiM_3)_{oct}O_8$ and *l*-$Li_{1/2}MO_2$ (M ≡ 3d TM) structures as well their delithiated counterparts *ps*-$(M)_{tet}(M_3)_{oct}O_8$ and *l*-MO_2.

Table 2 gives the calculated energy difference ($\Delta E_{oct\rightarrow tet}$) between *ps*-$(LiM)_{tet}(LiM_3)_{oct}O_8$ and *l*-$Li_{1/2}MO_2$ for the 3d transition metals from Ti to Cu (ordered lowest $\Delta E_{oct\rightarrow tet}$ to highest). It also lists the change in valence and d-orbital filling that accompanies the structural change from *l*-$Li_{1/2}MO_2$ to *ps*-$(LiM)_{tet}(LiM_3)_{oct}O_8$. The valence and d-orbital filling have been determined using spin integration as described in section 5. For each respective change in d-orbital filling that accompanies the formation of tetrahedral M, the projected change in LFSE and spin-paining energy (SPE) is given. The SPE is important to consider because the splitting from spin pairing (Δ_s) can be of comparable magnitude to the splitting from the ligand field in 3d transition metals (hence the existence of high-spin octahedral cations when $\Delta_s > \Delta_o$).[50,51] Δ_s is the additional repulsive

Table 2. Energy Differences between *ps*-$(LiM)_{tet}(LiM_3)_{oct}O_8$ and *l*-$Li_2M_4O_8$ (M ≡ 3d TM) for Each 3d TM from Ti to Cu Listed from Lowest ΔE to Highest[a]

reaction	$\Delta E_{oct\rightarrow tet}$ (eV)	*d* filling	Δ LFSE and SPE
$2Mn_{oct}^{3+} \rightarrow Mn_{oct}^{4+} + Mn_{tet}^{2+}$	−0.33	$2t_{2g}^3e_g^1 \rightarrow t_{2g}^3 + e^2t_2^3$	α
$4Fe_{oct}^{3.5+} \rightarrow Fe_{tet}^{3+} + 3Fe_{oct}^{3.67+}$	−0.17	$4t_{2g}^{41/2} \rightarrow e^2t_2^3 + 3t_{2g}^{41/3}$	$2\Delta_o - 2\Delta_s$
$Cu_{oct} \rightarrow Cu_{tet}$[b]	−0.15	NA	NA
$4Ti_{oct}^{3.5+} \rightarrow Ti_{tet}^{4+} + 3Ti_{oct}^{3.33+}$	−0.12	$4t_{2g}^{1/2} \rightarrow e^0t_2^0 + 3t_{2g}^{2/3}$	0
$V_{oct}^{3.5+} \rightarrow V_{tet}^{3.5+}$	0.039	$t_{2g}^{11/2} \rightarrow e^{11/2}$	$(3/5)\Delta_o - (9/10)\Delta_t$
$Cr_{oct}^{3.5+} \rightarrow Cr_{tet}^{3.5+}$	0.30	$t_{2g}^{21/2} \rightarrow e^2t_2^{1/2}$	$\Delta_o - \Delta_t$
$2Ni_{oct}^{3+} \rightarrow Ni_{oct}^{4+} + Ni_{tet}^{2+}$	0.43	$2t_{2g}^6e_g^1 \rightarrow t_{2g}^6 + e^4t_2^4$	$(6/5)\Delta_o - (4/5)\Delta_t + \alpha$
$4Co_{oct}^{3.5+} \rightarrow 3Co_{oct}^{4+} + Co_{tet}^{2+}$	0.58	$4t_{2g}^{51/2} \rightarrow 3t_{2g}^5 + e^4t_2^3$	$(14/5)\Delta_o - (6/5)\Delta_t - 2\Delta_s$

[a] Column 1 gives the valence states accompanying the movement of the TM ion from octahedral to tetrahedral coordination. Column 2 gives the energy difference between *ps*-$(LiM)_{tet}(LiM_3)_{oct}O_8$ and *l*-$Li_2M_4O_8$ per tetrahedral M. Column 3 holds the change in d-orbital filling that results from moving the TM ion from octahedral to tetrahedral coordination. The projected change in LFSE and spin pairing energy (SPE) that results from the change in d-orbital filling is listed in column 4. This energy is expressed in terms of the octahedral splitting (Δ_o), the tetrahedral splitting (Δ_t), the Jahn−Teller splitting (α), and the spin-pairing splitting (Δ_s). Δ_s is the additional repulsive energy from two electrons of opposing spin occupying the same d orbital. [b] The change in valence/d filling for Cu could not be determined using the method of section 5.

Table 3. Energy Differences between *ps*-$(M)_{tet}(M_3)_{oct}O_8$ and *l*-M_4O_8 (M ≡ 3d TM) for Each 3d TM from Ti to Cu Listed from Lowest ΔE to Highest[a]

reaction	$\Delta E_{oct\rightarrow tet}$ (eV)	*d* filling	Δ LFSE and SPE
$Cr_{oct}^{4+} \rightarrow Cr_{tet}^{4+}$	0.54	$t_{2g}^2 \rightarrow e^2$	$(4/5)\Delta_o - (6/5)\Delta_t$
$V_{oct} \rightarrow V_{tet}$[b]	0.57	NA	NA
$Ti_{oct}^{4+} \rightarrow Ti_{tet}^{4+}$	0.64	$t_{2g}^0 \rightarrow e^0$	0
$Fe_{oct} \rightarrow Fe_{tet}$[b]	0.76	NA	NA
$Cu_{oct} \rightarrow Cu_{tet}$[b]	1.0	NA	NA
$Co_{oct}^{4+} \rightarrow Co_{tet}^{4+}$	1.3	$t_{2g}^5 \rightarrow e^2t_2^3$	$2\Delta_o - 2\Delta_s$
$Mn_{oct}^{4+} \rightarrow Mn_{tet}^{4+}$	2.1	$t_{2g}^3 \rightarrow e^2t_2^1$	$(6/5)\Delta_o - (4/5)\Delta_t$
$Ni_{oct}^{4+} \rightarrow Ni_{tet}^{4+}$	2.6	$t_{2g}^6 \rightarrow e^3t_2^3$	$(12/5)\Delta_o - (3/5)\Delta_t - -2\Delta_s$

[a] Column 1 gives the valence states accompanying the movement of the TM ion from octahedral to tetrahedral coordination. Column 2 gives the energy difference between *ps*-$(M)_{Tet}(M_3)_{oct}O_8$ and *l*-M_4O_8 per tetrahedral M. Column 3 holds the change in d-orbital filling that results from moving the TM ion from octahedral to tetrahedral coordination. The projected change in LFSE and spin-pairing energy (SPE) that results from the change in d-orbital filling is listed in column 4. This energy is expressed in terms of the octahedral splitting (Δ_o), the tetrahedral splitting (Δ_t), and the spin-pairing splitting (Δ_s). [b] The change in valence/d filling for Cu, Fe, and V could not be determined using the method of section 5.

energy caused by two electrons of opposing spin occupying the same d orbital. For finding the change in SPE of Tables 2 and 3, Δ_s is assumed to be roughly equal for both octahedrally and tetrahedrally coordinated d orbitals. Table 3 contains the results from calculations on *ps*-$(M)_{tet}(M_3)_{oct}O_8$ and *l*-MO_2 for the 3d transition metals from Ti to Cu (ordered lowest $\Delta E_{oct\rightarrow tet}$ to highest).

Each 3d metal from Ti to Cu in Table 2 and 3 will now be discussed.

10.1. Ti

Ti is calculated to have a delocalized d band in *l*-$Li_{1/2}TiO_2$. This is reflected by each Ti holding a +3.5 charge. In *l*-TiO_2, Ti is calculated to have an empty d band and a +4 valence. At both Li concentrations the tetrahedral Ti is +4 and the projected change in LFSE and SPE for Ti moving from octahedral to tetrahedral coordination is zero. This is consistent with Ti having a relatively low calculated value for $\Delta E_{oct\rightarrow tet}$ (fourth lowest in Table 2 and third lowest in Table 3).

However, the that fact $\Delta E_{oct\rightarrow tet}$ for Ti is higher than Mn and Fe in Table 2 and higher than Cr in Table 3 runs contrary to expectations based solely on LFSE and SPE since Mn and Fe at $X_{Li} = 1/2$ and Cr at $X_{Li} = 0$ have a projected change in LFSE and SPE that is greater than zero.

If *l*-Li_xTiO_2 could be synthesized, the negative value of $\Delta E_{oct\rightarrow tet}$ for $Li_{1/2}TiO_2$ (−0.12 eV) suggests that Ti in a layered structure could be susceptible to migration into the Li layer at partial lithiation. Experimentally layered $LiTiO_2$ has not been synthesized as the similar ionic size between Li and Ti leads to a disordered rock-salt structure.[61] Layered $Li(Ni_{0.45}Ti_{0.55})O_2$ has been synthesized; however, it suffers from poor cyclability which is blamed on Ti migration into the Li/vacancy layer.[62] Additionally, Ti has been reported to migrate into the Na layer of layered $NaTiO_2$.[63] These experimental observations are consistent with the relative ease Ti^{4+} is expected to have in moving between octahedral and tetrahedral coordination due to a lack of ligand-field stabilization.

10.2. V

At $X_{Li} = 1/2$, V is calculated to maintain the same valence (+3.5) in octahedral and tetrahedral coordination, i.e., there is no charge disproportionation in forming tetrahedral V at this Li composition (Table 2). The projected change in LFSE and SPE at $X_{Li} = 1/2$ is $(3/5)\Delta_o - (9/10)\Delta_t$, which is positive whether the proportionality given by crystal-field theory $|4/9\Delta_o| = |\Delta_t|$ is assumed[46] or if $\Delta_t \approx 0$ is assumed as the results in section 8 suggest for Mn. The greater change in LFSE and SPE for $Li_{1/2}VO_2$ than for $Li_{1/2}TiO_2$ is consistent with a greater value of $\Delta E_{oct\rightarrow tet}$ in Table 2. This suggests that V should be less prone than Ti to enter tetrahedral sites at this average valence, and hence *l*-$Li_{1/2}VO_2$ should be more resistant against transformation than *l*-$Li_{1/2}TiO_2$. How-

ever, $\Delta E_{oct\rightarrow tet}$ is still relatively small (0.039 eV/V_{tet}), suggesting that V might still easily migrate out of metastable octahedral sites at this composition.

The value of $\Delta E_{oct\rightarrow tet}$ for VO_2 was calculated to be the second lowest in Table 3. Unfortunately the valences of V in *ps*-$(M)_{tet}(M_3)_{oct}O_8$ could not be clearly determined using the spin integration method of section 5 because the net spin on the V did not match a spin-polarized configuration consistent with the average formal oxidation state. Instead, the V took on a non-spin-polarized state.

10.3. Cr

Like V, Cr is calculated to maintain a +3.5 oxidation state in both octahedral and tetrahedral coordination at $X_{Li} = 1/2$ (Table 2). At this lithium concentration the projected change in LFSE and SPE is higher for Cr than for V, which is consistent with the greater value of $\Delta E_{oct\rightarrow tet}$ calculated for Cr in Table 2. This supports Cr having a stronger preference for octahedral sites at the +3.5 valence than V. At +4 valence Cr was calculated to have the lowest $\Delta E_{oct\rightarrow tet}$ in Table 3. This is consistent with the relatively low projected change in LFSE and SPE for Cr^{4+} moving from octahedral to tetrahedral coordination ($(4/5)\Delta_o - (6/5)\Delta_t$).

The enhanced stability of *l*-$Li_x(Cr_{1/2}Mn_{1/2})O_2$ reported experimentally can be explained by these results.[53] As *l*-$Li(Cr_{1/2}Mn_{1/2})O_2$ is delithiated, the Mn is oxidized to +4 first according to section 9 and experiment.[55] As already discussed, Mn^{4+} is highly stable in octahedral coordination. Cr is oxidized to +4 later in the charge, when Li vacancies that can facilitate TM ion migration are more plentiful. The relatively high value of $\Delta E_{oct\rightarrow tet}$ calculated for $Cr^{3.5+}$ in Table 2 probably reflects a strong preference for octahedral coordination at this valence. One would expect Cr to have an even stronger preference for octahedral coordination in *l*-$Li_{1/2}(Cr_{1/2}Mn_{1/2})O_2$ since its valence is +3 which has a t_{2g}^3 orbital filling—the same orbital filling as Mn^{4+}.

While Cr^{4+} has the lowest $\Delta E_{oct\rightarrow tet}$ in Table 3 and relatively weak ligand-field stabilization, the absolute value of $\Delta E_{oct\rightarrow tet}$ (0.54 eV) for CrO_2 is still higher than that for $Li_{1/2}CrO_2$ (0.3 eV). Furthermore, there probably is no longer a driving force to convert to spinel in highly delithiated *l*-$Li_x(Cr_{1/2}Mn_{1/2})O_2$. The fact that the structural integrity of *l*-$Li_x(Cr_{1/2}Mn_{1/2})O_2$ is maintained over delithiation attests to a relatively strong octahedral site preference exhibited by Cr at partial lithiation.

It has been observed that when Cr^{6+} is formed in delithiated *l*-$Li(Li_{1/5}Mn_{2/5}Cr_{2/5})O_2$, it spontaneously moves into tetrahedral coordination.[55] This is consistent with the lack of d electrons for Cr^{6+} and hence the lack of ligand-field stabilization.

10.4. Mn

Mn goes from having the lowest $\Delta E_{oct\rightarrow tet}$ at $X_{Li} = 0.5$ (Table 2) to the second highest $\Delta E_{oct\rightarrow tet}$ at $X_{Li} = 0$ (Table 3). The low value of $\Delta E_{oct\rightarrow tet}$ for Mn at $X_{Li} = 0.5$ is consistent with a relatively small projected change in LFSE and SPE equal to the Jahn−Teller splitting (α).[47,48]

As mentioned before, the fact that $\Delta E_{oct\rightarrow tet}$ is lower for Mn than for Ti despite α being greater than zero runs contrary to expectations based solely on LFSE. According to the simple model of eqs 3−5 in section 8.1, the low energy of *ps*-$(LiMn)_{tet}(LiMn_3)_{oct}O_8$ compared to *l*-$Li_{1/2}MnO_2$ can be explained by a lower d barycenter in *ps*-$(LiMn)_{tet}(LiMn_3)_{oct}O_8$ (eq 6). The d electrons of the tetrahedral Mn^{2+} enter d orbitals that are shifted lower in energy, probably because they are surrounded by less negative charge in a tetrahedral site than in an octahedral one. Ti^{4+}, on the other hand does not have any d electrons, so there is no energy reduction resulting from a lower tetrahedral d barycenter.

Another factor that could make $\Delta E_{oct\rightarrow tet}$ particularly low for Mn in Table 2 is the half-full orbital shells of Mn^{2+} and Mn^{4+} (the products of Mn^{3+} charge disproportionation). In general, half-full or full orbital shells have lower energy than other fillings because the electron−electron repulsion is decreased[64] (this is why in the chemistry of low atomic number elements the electrons arrange so often to produce full "octets"). On this basis one expects Mn^{2+} to have a lower electron−electron repulsion energy due to its half-full d shell[64] ($e^2t_2^3$ in tetrahedral coordination). It is also favorable for the levels that result from ligand-field splitting to be half-full or full.[50] Therefore, the half-full t_{2g} level (t_{2g}^3) of Mn^{4+} is favorable in this regard as well. The energetic favorability of half-filled levels is another reason Mn^{3+} in many environments is observed to be unstable to both reduction to Mn^{2+} and oxidation to Mn^{4+}.[52]

10.5. Fe

At $X_{Li} = 0.5$ there is a large positive change in LFSE ($2\Delta_o$) for the formation of tetrahedral Fe. However, this is counteracted by a large negative change in spin-pairing energy ($-2\Delta_s$). The decrease in spin-pairing energy is caused by one of the low-spin $Fe_{oct}^{2/3+}$ becoming high-spin Fe_{tet}^{3+}. Recalling that Δ_s can be comparable in magnitude to Δ_o in 3d metal oxides,[50,51] the net change in LFSE and SPE given for Fe in Table 2 is probably small. This is consistent with the negative value calculated for $\Delta E_{oct\rightarrow tet}$ (−0.17 eV/Fe tet). However, the net change in LFSE and SPE should still have a positive value since Fe is calculated to be low spin in octahedral coordination ($t_{2g}^{4.5}$ or $t_{2g}^{4.33}$), indicating that $|\Delta_s| < |\Delta_o|$.

l-$LiFeO_2$ has been synthesized by ion exchange from $NaFeO_2$, but it shows little or no electrochemical activity.[65] It was not reported whether this is a result of Fe^{3+} migration; however, the results of Table 2 suggest that Fe should be susceptible to migration out of the TM layer at partial lithiation in *l*-Li_xFeO_2

At $X_{Li} = 0$ Fe was found to be of intermediate stability in octahedral coordination. Unfortunately the valences of the Fe ions could not be clearly determined using the spin integration method of section 5 because the net spin on the Fe did not match a high-spin or low-spin configuration consistent with the average formal oxidation state (+4). This suggests that the d-orbital filling takes on an

intermediate spin configuration for Fe and/or the assumed oxygen formal oxidation state of −2 is no longer justified due to strong covalency between the Fe and O.

10.6. Co

Co has the highest value of $\Delta E_{oct\rightarrow tet}$ in Table 2. This is consistent with it having the largest projected change in LFSE ($(14/5)\Delta_o - (6/5)\Delta_t$). However, the change in LFSE is somewhat counteracted by a negative change in spin-pairing energy ($-2\Delta_s$). The spin-pairing energy is reduced in the charge disproportionation of Co where four d fillings of $t_{2g}^{5.5}$ change to three t_{2g}^5 and $e^4t_2^3$. This helps explain why $\Delta E_{oct\rightarrow tet}$ calculated for Co is not as high compared to the other 3d metals as one would expect on the basis of LFSE alone.

At $X_{Li} = 0$ Co has the third highest $\Delta E_{oct\rightarrow tet}$. Its change in LFSE and SPE is $2\Delta_o - 2\Delta_s$ and the same as Fe at $X_{Li} = 0.5$, which has a low $\Delta E_{oct\rightarrow tet}$. A possible explanation for this is that the magnitude of Δ_o is higher and/or the magnitude of Δ_s is lower for Co^{4+} than for $Fe^{3.5+}$.

The remarkable success of $LiCoO_2$ as an electrode material is likely related to the strong intrinsic preference of Co for octahedral sites over the +3 to +4 valences as indicated by the high calculated value of $\Delta E_{oct\rightarrow tet}$ in Tables 2 and 3. This strong preference of Co for octahedral sites clearly suggests that Co will not easily migrate through an close-packed oxygen framework at these oxidation states.

10.7. Ni

Ni is calculated to have the second highest $\Delta E_{oct\rightarrow tet}$ at $X_{Li} = 0.5$ and the highest $\Delta E_{oct\rightarrow tet}$ at $X_{Li} = 0$. At $X_{Li} = 0.5$, Ni is calculated to undergo a charge disproportionation reaction (eq 1) similar to Mn and Co. The projected change in LFSE and SPE is higher for Ni than Cr, which is consistent with the higher value of $\Delta E_{oct\rightarrow tet}$ calculated for Ni than Cr in Table 2. On the basis of these calculations, Ni is expected to be the second most stable in octahedral sites at an average valence of +3.5 of the 3d metals from Ti to Cu.

The high value of $\Delta E_{oct\rightarrow tet}$ calculated for Ni at $X_{Li} = 0$ is consistent with the large projected change in LFSE ($12/5\Delta_o - 3/5\Delta_t$). However, as with $Co^{3.5+}$, the change in LFSE is somewhat counteracted by a negative change in spin-pairing energy ($-2\Delta_s$), which helps explain why $\Delta E_{oct\rightarrow tet}$ calculated for Ni^{4+} is not as high compared to the other 3d metals as one would expect on the basis of LFSE alone.

The calculated stability of Ni in octahedral coordination is consistent with the good electrochemical performance observed experimentally for Li(MnNi)O_2 compounds. The Ni^{2+} oxidizes Mn to +4, which as already discussed has a strong preference for octahedral sites. When the average valence of Ni is between +3 and +4, there is a high concentration of Li vacancies that would facilitate ion migration, except for the strong preference of Ni for octahedral sites over this valence range. Ni^{2+} also most likely has a strong preference for octahedral coordination due to ligand-field effects, although probably not as strong as Ni^{3+} since there is an additional electron in the e_g level.

10.8. Cu

At an average formal valence of +3.5, Cu is calculated to have the third lowest $\Delta E_{oct\rightarrow tet}$ equal to −0.15 eV per tetrahedral Cu. This suggests that Cu at this average valence does not have a strong preference for octahedral sites. At an average formal valence of +4, $\Delta E_{oct\rightarrow tet}$ for Cu (1 eV) is ranked fourth highest in Table 3. In practice, such high oxidation states for Cu are probably difficult to achieve. However, if it were to occur, a metastable structure like l-Li_xCuO_2 should be prone to transformation at partial lithiation according to these results. Unfortunately, the valence of Cu in both cases could not be clearly determined using the spin integration method of section 5.

10.11. Overall Trends for 3d Metals

The energy of all the 3d metals entering tetrahedral coordination from the l-Li_xMO_2 structure decreases as X_{Li} goes from 0 to 1/2. This is similar to the defect calculations on Co and Mn in section 4 that found tetrahedral defect energies in the layered structure to decrease for both as Li content increases from 0 to 1/2.

At $X_{Li} = 0.5$, three of the eight TM ions (Mn, Co, and Ni) were found to undergo a major charge disproportionation reaction (eq 1) when moved from octahedral to tetrahedral coordination. In contrast, at $X_{Li} = 0$ none were found to undergo charge disproportionation.

Table 2 shows a good correlation between the relative energetics of octahedral and tetrahedral site occupancy by a 3d metal ion and the projected change in LFSE for moving a 3d metal ion from octahedral to tetrahedral coordination. From rows 4 (Ti) to 8 (Co) in Table 2 the correlation is perfect; the value calculated for $\Delta E_{oct\rightarrow tet}$ increases along with the projected change in LFSE (from 0 for Ti to $(14/5)\Delta_o - (6/5)\Delta_t$ for Co).

The two deviations from this trend are Mn and Fe, which have the two most negative values for $\Delta E_{oct\rightarrow tet}$. Both of these cases probably have relatively small net changes in LFSE and SPE, which is consistent with a more general association between low values of $\Delta E_{oct\rightarrow tet}$ and low projected changes in LFSE and SPE. The case of Fe illustrates that focusing exclusively on LFSE can be misleading when spin pairing is present, especially in low-spin cations.

Table 3 also shows a good correlation between $\Delta E_{oct\rightarrow tet}$ and the projected change in LFSE, with the largest changes in LFSE being associated with the highest values of $\Delta E_{oct\rightarrow tet}$.

The results given in Tables 2 and 3 support the decisive role of LFSE in the site preference and most likely the mobility of 3d metal ions in a ccp lattice. For Mn, Ni, and Co the results in Table 2 are consistent with the experimental work of Choi, Manthiram et al. who found increasing resistance of l-Li_xMO_2 against transformation into spinel as M is

changed from Mn to Ni to Co.[49] Table 2 shows that $\Delta E_{oct \rightarrow tet}$ and the projected change in LFSE and SPE for Ni fall between those values for Mn and Co; this agrees with the observed intermediate stability of *l*-Li_xNiO_2 compared to *l*-Li_xMnO_2 and *l*-Li_xCoO_2.

11. Conclusions

For phase transformations involving rearrangement of transition-metal cations over octahedral sites within a fixed ccp oxide framework, such as the transformation of layered Li_xMnO_2 to spinel, the results of this study indicate that the low-energy pathway for transition-metal migration between octahedral sites is through a shared nearest neighbor tetrahedral site (i.e., $O_h \rightarrow T_d \rightarrow O_h$) rather than directly between octahedral sites ($O_h \rightarrow O_h$). This suggests that the smaller the energy change is for transition-metal ion movement between octahedral and tetrahedral coordination, the more easily the TM ions should be able to rearrange in a ccp oxide when transforming from a metastable structure to a stable one. As a result, the resistance against transformation of metastable transition-metal oxides with a ccp oxygen sublattice (e.g., Li_xMnO_2 with α-$NaFeO_2$ structure) will depend on the relative stability of the transition metal in octahedral coordination compared to tetrahedral coordination. The availability of empty tetrahedra without any cations occupying nearest neighbor face-sharing octahedra is also an important factor in the ability of TM ions to migrate through a ccp oxide. Such tetrahedra provide a relatively low-energy pathway by avoiding the highly repulsive interaction between face-sharing cations.

The energetics of Mn movement between octahedral and tetrahedral sites is found to be particularly sensitive to valence. Of the 3d transition metals from Ti to Cu, Mn is calculated to be the second most stable in octahedral coordination at +4 valence and the least stable at +3 valence. This appears to result from a large difference in ligand-field stabilization between the +4 to +3 states of charge for Mn. The most unfavorable change in LFSE associated with Mn movement from octahedral to tetrahedral coordination occurs when Mn is +4 with three spin-polarized d electrons occupying a half-filled t_{2g} shell in octahedral coordination. In contrast, Mn_{oct}^{3+} ($t_{2g}^3e_g^1$) is calculated to undergo a charge disproportionation reaction (eq 1), forming Mn_{tet}^{2+} ($e^2t_2^3$) and Mn_{oct}^{4+} (t_{2g}^3), which allows Mn^{2+} movement into tetrahedral coordination with a relatively low change in LFSE.

The low-energy passage of Mn through tetrahedral sites enabled by Mn_{oct}^{3+} charge disproportionation appears to underlie the instability of metastable ccp Mn oxides such as the layered α-$NaFeO_2$ and orthorhombic structures with electrochemical cycling. In both of these structures Mn_{oct}^{3+}, which can charge disproportionate, and Li vacancies, which facilitate Mn migration by providing empty tetrahedral sites without face-sharing cations, coexist over the Li concentration range where these structures are not thermodynamically stable.

Spinel-like $Li_xMn_2O_4$, on the other hand, maintains its structural integrity, even when it is not thermodynamically stable at high and low lithium content. This is probably because significant amounts of Mn^{3+} and Li vacancies do not coexist over ranges of Li concentration where the spinel-like structure is metastable. At low lithium concentrations the Mn are primarily in the +4 oxidation state and consequently have relatively low mobility. At high Li content ($x \approx 2$ in $Li_xMn_2O_4$) there are insufficient Li vacancies to allow easy Mn rearrangement. When substantial concentrations of Mn^{3+} and Li vacancies coexist in *s*-$LiMn_2O_4$, the spinel structure is thermodynamically stable and hence not adversely effected by the increased mobility of Mn. However, there still is the problem of Mn dissolution into the electrolyte through Mn^{3+} charge disproportionation.

LFSE also appears to be a decisive factor in the site preference of other 3d TM ions in a ccp oxide. As with Mn, this should impact the resistance of other metastable 3d TM oxides against transformation. The resistance against transformation imparted by ligand-field effects appears to be epitomized in the case of layered Li_xCoO_2. Contrary to the case with Mn, the change in LFSE associated with Co movement from octahedral to tetrahedral coordination is highly unfavorable in $Li_{1/2}CoO_2$. This provides impressive stability for layered Li_xCoO_2 with electrochemical cycling over Li concentrations where the spinel structure is thermodynamically stable (e.g., $Li_{1/2}CoO_2$).

The results of this investigation lead to the prediction that, in general, metastable Mn oxide structures with a ccp oxygen sublattice will rapidly transform to stable ccp structures if Mn^{3+} and/or Mn^{2+} coexist with sufficient vacant interstitial sites. This is due to the lack of ligand-field stabilization for Mn_{oct}^{2+} and the susceptibility of Mn_{oct}^{3+} to charge disproportionation, which results in low ligand-field stabilization. This in turn makes tetrahedral sites relatively accessible to Mn, which facilitates cationic rearrangement.

The energy difference between oxide structures with and without Mn in tetrahedral coordination can be fitted reasonably well to a simple model in which the energy difference is broken down into two contributions. One contribution is independent of Mn d-orbital filling and hence Mn valence. It accounts for the change in interaction energy between a Mn^{7+} (i.e., d^0) ionic core and the surrounding cations as a Mn moves from an octahedral to a tetrahedral site. The other energy contribution is from the changing energy of the filled d orbitals as Mn is moved from octahedral to tetrahedral coordination. The latter energy contribution varies in a piecewise linear fashion with Mn valence and has a peak at Mn^{4+}, reflecting the ligand-field splitting of octahedrally and tetrahedrally coordinated d orbitals.

The energy contribution from the changing Mn d orbitals as Mn moves from octahedral to tetrahedral coordination can in turn be separated into the change of the Mn d-orbital energy barycenter and the change in ligand-field stabilization energy. While the change in LFSE is determined by the Mn valence, the d-orbital barycenter and the energy of interactions involving the Mn^{7+} ionic cores are found to be much more sensitive to cationic ordering.

Using ionic valences found through a large series of calculations on substituted Mn oxides, a qualitative ionization scale between Mn and other 3d metals has been constructed. This scale allows one to predict the valences for Mn (in octahedral and/or tetrahedral coordination) coexisting with another 3d TM cation (in octahedral coordination) in a ccp oxide. This could be useful for designing TM oxide materials with improved kinetic stability over the range of Li concentrations covered by electrochemical cycling.

The findings of this study point to a number of different strategies for producing lithium manganese oxide structures, other than spinel, that resist transformation with electrochemical cycling. If a metastable ccp oxide structure such as *l*-Li_xMnO_2 or *o*-Li_xMnO_2 ($X_{Li} < 1$) is used, high concentrations of Mn_{oct}^{3+} and Li vacancies should be prevented from coexisting over regions of metastability. This can be accomplished by chemically substituting for Mn with low fixed valence and/or electronegative multivalent cations that can oxidize the Mn e_g orbital. There are many different examples of this approach that have had some success experimentally.[7,18,53−55] Another way of oxidizing the Mn e_g orbital is to introduce vacancies into the Mn sublattice.[66]

Given that Mn^{4+} is the most stable valence in octahedral coordination, it might be desirable for Mn to be electrochemically cycled between elevated oxidation states centered closer to +4 rather than over the +3/+4 redox range characteristic of Li_xMnO_2 structures. Unfortunately at this time there probably are not any electrolytes that can withstand the oxidative strength of Mn at valences higher than +4.[67] An additional problem with Mn charged above +4 in ccp oxides is the possibility of decomposition reactions producing O_2.[58,68]

Another strategy is to use a structure with an oxygen sublattice that is different from that of spinel (i.e., non-ccp). For such a structure to transform into spinel the oxygen needs to rearrange, which should make the transformation much more difficult.

One way this has been accomplished experimentally is by using a close-packed oxide structure that is not *cubic*-close packed.[69,70] Such structures may be more resistant against transformation to spinel, but there still is a network of octahedral and tetrahedral sites that could possibly allow undesirable Mn movement during electrochemical cycling. The phospho-olivine structure is an example of a non-ccp oxide that has shown good reversible capacity with iron ($LiFePO_4$) however not with Mn (although Mn combined with Fe is reported to perform well).[71] Oxides containing polyanions such as PO_4^{-3} offer a rich diversity of structures that might be suitable for use in a positive electrode.[72]

Another option is to use a non-close-packed structure. A more open structure can constrain Mn by eliminating energetically favorable sites it can migrate through (e.g., tetrahedral sites). A layered structure can be made less close packed by pillaring open the Li/vacancy layer with a large cation like K^+ or with a cluster of atoms.[73] The tunneled Mn oxides are another example of non-close-packed structures. Good cyclability and resistance against transformation to spinel has been achieved by Doeff et al. using such a structure.[74,75]

12. Acknowledgments

This research was supported in part by the MRSEC Program of the National Science Foundation under award number DMR-02-13282 and by the Assistant Secretary for Energy Efficiency and Renewable Energy, Office of Freedom CAR and Vehicle Technologies, of the U.S. Department of Energy under Contract No. DE-AC03-76SF00098, Subcontract No. 6517748 with the Lawrence Berkeley National Laboratory. Methodological developments that made this work possible have been supported by the Department of Energy under contract number DE-FG02-96ER45571. NPACI is acknowledged for providing substantial computing resources for this work. G.C. acknowledges a faculty development chair from R. P. Simmons.

13. References

(1) Mizushima, K.; Jones, P. C.; Wiseman, P. J. *Solid State Ionics* **1981**, *3−4* (Aug), 171.
(2) Thackeray, M. *Prog. Solid State Chem.* **1997**, *25*, 1.
(3) Winter, M.; Besenhard, J.; Spahr, M.; Novak, P. *Adv. Mater.* **1998**, *10*, 725.
(4) Bruce, P. *Chem. Commun.* **1997**, 1817.
(5) Armstrong, A. R.; Bruce, P. G. *Nature* **1996**, *381*, 499.
(6) Capitaine, F.; Gravereau, P.; Delmas, C. *Solid State Ionics Diffusion React.* **1996**, *89*, 197.
(7) Armstrong, A.; Robertson, A.; Bruce, P. *Electrochem. Acta* **1999**, *45*, 285.
(8) Bruce, P.; Armstrong, A.; Gitzendanner, R. *J. Mater. Chem.* **1999**, 193.
(9) Shao-Horn, Y.; Hackney, S. A.; Armstrong, A. R.; Bruce, P. G.; Gitzendanner, R.; Johnson, C. S.; Thackeray, M. M. *J. Electrochem. Soc.* **1999**, *146*, 2404.
(10) Armstrong, A.; Robertson, A.; Gitzendanner, R.; Bruce, P. *J. Solid State Chem.* **1999**, *145*, 549.
(11) Broussely, M.; Biensan, P.; Simon, B. *Electrochem. Acta* **1999**, *45*, 3.
(12) Van der Ven, A.; Ceder, G. *Phys. Rev. B* **1999**, *59* (2), 742.
(13) Ceder, G.; Van der Ven, A. *Electrochem. Acta* **1999**, *45* (1−2), 13150.
(14) Blyr, A.; Sigala, C.; Amatucci, G.; Guyomard, D.; Chabre, Y. *J. Electrochem. Soc.* **1998**, *145*, 194.
(15) Chiang, Y. M.; Sadoway, D. R.; Jang, Y. I.; Huang, B.; Wang, H. *Electrochem. Solid State Lett. 2* **1999**, *3*, 107.
(16) Vitins, G.; West, K. *J. Electochem. Soc.* **1997**, *144*, 2587.
(17) Chiang, Y.-M.; Wang, H.; Jang, Y. *Chem. Mater.* **2001**, *13*, 53.
(18) Wang, H.; Jang, Y.; Chiang, Y.-M. *Electrochem. Solid State Lett.* **1999**, *2* (10), 490.
(19) Hunter, J. C. *J. Solid State Chem.* **1981**, *39*, 142
(20) David, W. I. F.; Thackeray, M. M.; Bruce, P. G.; Goodenough, J. B. *Mater. Res. Bull.* **1984**, *19*, 99.
(21) Wang, H.; Jang, Y.-I.; Huang, B.; Sadoway, D. R.; Chiang, Y.-M. *J. Electrochem. Soc.* **1999**, *146*, 473.
(22) Gabrisch, H.; Yazami, R.; Fultz, B. *J. Power Sources* **2003**, *119*, 674.
(23) Van der Ven, A.; Ceder, G. *Electrochem. Solid State Lett.* **2000**, *3* (7).
(24) Reed, J. Ab Initio Study of Cathode Materials for Lithium Batteries. Ph.D. Thesis, M.I.T., 2003; p 65.
(25) Parr, R. G.; Yang, W. *Density-Functional Theory of Atoms and Molecules*; Oxford University Press: New York, 1989; pp 51−52.
(26) Parr, R. G.; Yang, W. *Density-Functional Theory of Atoms and Molecules*; Oxford University Press: New York, 1989; pp 142−145.
(27) Ohno, K.; Esfarjani, K.; Kawazoe, Y. *Computational Materials Science*; Springer-Verlag: Berlin, Heidelberg, 1999; pp 21−25.
(28) Mishra, S. K.; Ceder, G. *Phys. Rev. B* **1999**, *59*, 6120.
(29) Van der Ven, A.; Aydinol, M. K.; Ceder, G. *J. Electrochem. Soc.* **1998**, *145* (6), 2149.
(30) Kresse, G.; Furthmuller, J. *Phys. Rev. B* **1996**, *54* (11), 169.
(31) Parr, R. G.; Yang, W. *Density-Functional Theory of Atoms and Molecules*; Oxford University Press: New York, 1989; pp 153 and 154.

(32) Ohno, K.; Esfarjani, K.; Kawazoe, Y.; *Computational Materials Science*; Springer-Verlag: Berlin, Heidelberg, 1999; pp 106 and 107.
(33) Vanderbilt, D. *Phys. Rev. B* **1990**, *41*, 7892.
(34) Mizushima, K.; Jones, P. C.; Wiseman, P. J.; Goodenough, J. B. *Mater. Res. Bull.* **1980**, *15*, 783.
(35) Orman, H. J.; Wiseman, P. J. *Acta Crystallogr., Sect. C* **1984**, *139*, 12.
(36) Ceder, G.; Van der Ven, A. *Electrochim. Acta* **1999**, *45*, 131.
(37) Wolverton, C.; Zunger, A. *J. Electrochem. Soc.* **1998**, *145*, 2424.
(38) Gummow, R.; Liles, D. C.; Thackeray, M. M. *Mater. Res. Bull.* **1993**, *28*, 1249.
(39) Reed, J.; Ceder, G.; Van der Ven, A. *Electrochem. Solid State Lett.* **2001**, *4* (6), A78.
(40) Reed, J.; Ceder, G. *Electrochem. Solid State Lett.* **2002**, *5* (7), A145.
(41) Borg, R. J.; Dienes, G. J. *The Physical Chemistry of Solids*; Academic Press: New York, 1992; pp 148−152.
(42) Burns, R. G. *Mineralogical Applications of Crystal Field Theory*; Cambridge University Press: New York, 1970, 1993; p 464.
(43) Goodenough, J. B.; Loeb, A. L. *Phys. Rev.* **1955**, *l98*, 391.
(44) Figgis, B. N.; Hitchman, M. A. *Mineralogical Applications of Crystal Field Theory*; Wiley-VCH: New York, 2000; p 116.
(45) Burns, R. G. *Mineralogical Applications of Crystal Field Theory*; Cambridge University Press: New York, 1970, 1993; p 17.
(46) Burns, R. G. *Mineralogical Applications of Crystal Field Theory*; Cambridge University Press: New York, 1970, 1993; p 22.
(47) Burns, R. G. *Mineralogical Applications of Crystal Field Theory*; Cambridge University Press: New York, 1970, 1993; p 218.
(48) Burns, R. G. *Mineralogical Applications of Crystal Field Theory*; Cambridge University Press: New York, 1970, 1993; p 231.
(49) Choi, S.; Manthiram, S. *J. Electrochem. Soc.* **2002**, *149* (9), A1157.
(50) Figgis, B. N.; Hitchman, M. A. *Mineralogical Applications of Crystal Field Theory*; Wiley-VCH: New York, 2000; pp 166−177.
(51) Burns, R. G. *Mineralogical Applications of Crystal Field Theory*; Cambridge University Press: New York, 1970, 1993; p 433.
(52) Burns, R. G. *Mineralogical Applications of Crystal Field Theory*; Cambridge University Press: New York, 1970, 1993; p 18.
(53) Davidson, I. J.; McMillan, R. S.; Slegr, J.; Luan, B.; Kargina, I.; Murray, J. J.; Swainson, I. P. *J. Power Sources* **1999**, *81−82*, 406.
(54) Rossen; Jones, C. D. W.; Dahn, J. R. *Solid State Ionics* **1992**, *57*, 311.
(55) Ammundsen, B.; Paulsen, J. *Adv. Mater.* **2001**, *13*, 943.
(56) Ammundsen, B.; Desilvestro, J.; Groutso, T.; Hassell, D.; Metson, J. B.; Regan, E.; Steiner, R.; Pickering, P. J. *J. Electrochem. Soc.* **2000**, *147*, 4078.
(57) de Groot, F. M. F.; Grioni, M.; Fuggle, J. C.; Ghigsen, J.; Sawatzky, G. A.; Petersen, H. *Phys. Rev. B* **1989**, *40*, 5715.
(58) Lu, Z.; Dahn, J. R. *J. Electrochem. Soc.* **2002**, *149* (7) A815.
(59) Park, H.-S; Hwang, S.-J.; Choy, J.-H. *J. Phys. Chem. B* **2001**, *105*, 4860.
(60) Burns, R. G. *Mineralogical Applications of Crystal Field Theory*; Cambridge University Press: New York, 1970, 1993; p 436.
(61) Chang, S. H.; Kang, S. G.; Song, S. W.; Yoon, J. B.; Choy, J. H. *Solid State Ionics* **1996**, *86−88*, 171.
(62) Kang, K.; Carlier, D.; Reed, J.; Arroyo, E.; Ceder, G.; Croguennec, L.; Delmas, C. *Chem. Mater.* **2003**, *15*, 4503.
(63) Maazaz, A.; Delmas, C.; Hagenmuller, P. *J. Inclusion Phenom.* **1983**, *1*, 45.
(64) Bethe, H.; Jackiw, R. *Intermediate Quantum Mechanics*; Addison-Wesley Longman, Inc.: New York, 1986, 1997; pp 80 and 81.
(65) Kanno, R.; Shirane, T.; Inaba, Y.; Kawamoto, Y. *J. Power Sources* **1997**, *68* (1), 145.
(66) Raekelboom, E. A.; Hector, A. L.; Owen, J.; Vitins, G.; Weller, M. T. *Chem. Mater.* **2001**, *13* (12), 4618.
(67) Robertson, A. D.; Bruce, P. G. *Chem. Commun.* **2002**, *23*, 2790.
(68) Lu, Z.; Beaulieu, L. Y.; Donaberger, R. A.; Thomas, C. L.; Dahn, J. R. *J. Electrochem. Soc.* **2002**, *149* (7) A815.
(69) Paulsen, J. M.; Larcher, D.; Dahn, J. R. *J. Electrochem. Soc.* **2000**, 147 (8), 2862.
(70) Eriksson, T. A.; Lee, Y. J.; Hollingsworth, J.; Reimer, J. A.; Cairns, E. J.; Zhang, X.-F.; Doeff, M. M. *Chem. Mater.* **2003**, *15*, 4456.
(71) Padhi, A. K.; Nanjundaswamy, K. S.; Goodenough, J. B. *J. Electrochem. Soc.* **1997**, *144* (4), 1188.
(72) Patoux, S. Matériaux d' électrode positive à charpente polyanionique pour batteries au lithium: Approches cristallochimiques et électrochimiques. Thése de Doctorat, L'Universite de Picardie Jules Verne, 2003.
(73) Zhang, F.; Ngala, K.; Whittingham, M. S. *Electrochem. Commun.* **2000**, *2*(6) 445.
(74) Doeff, M. M.; Richardson, T. J.; Kepley, L. *J. Electrochem. Soc.* **1996**, *143*(8), 2507.
(75) Doeff, M. M.; Anapolsky, A.; Edman, L.; Richardson, T. J.; De Jonghe, L. C. *J. Electrochem. Soc.* **2001**, *148* (3), A230.
(76) Reed, J. Ab Initio Study of Cathode Materials for Lithium Batteries. Ph.D. Thesis, M.I.T., 2003; pp 78−85.
(77) Reed, J. Ab Initio Study of Lithium Manganese Oxides. M.S. Thesis, M.I.T., 2001; pp 49−57.
(78) Reed, J. Ab Initio Study of Cathode Materials for Lithium Batteries. Ph.D. Thesis, M.I.T., 2003; pp 152−161.
(79) Reed, J. Ab Initio Study of Cathode Materials for Lithium Batteries. Ph.D. Thesis, M.I.T., 2003; pp 235−236.

CR020733X